NUMERICAL SIMULATION OF ISOTHERMAL GAS-LIQUID BUBBLY FLOW: INFLUENCE OF BUBBLE COALESCENCE AND BREAKUP

A THESIS SUBMITTED TO THE DEPARTMENT OF

NUCLEAR ENGINEERING

In Partial Fulfillment of the Requirements for the Degree of

MASTER OF PHILOSOPHY

COLLEGE OF BASIC AND APPLIED SCIENCES

UNIVERSITY OF GHANA

BY

(Castro Owusu-Manu Kwabena)

BSc (KNUST), 2010

In

NUCLEAR ENGINEERING

July, 2015

DECLARATION

I hereby certified that the work presented in this thesis is to the best of my knowledge and belief, original except where acknowledgement has been made; the material has not been submitted previously, either in whole or in part, for a degree at this or any other university.

…… ……

CASTRO OWUSU-MANU KWABENA Date

(Candidate)

I hereby declare that the preparation of this thesis work was supervised in accordance with the guidelines laid down by the University of Ghana.

…… ……

Dr StephenYamoah Emeritus Prof E.H.K Akaho

Date: Date:

DEDICATION

This research is dedicated to my mother Evelyn Norgbey for her guidance, and prayer support.

ACKNOWLEDGEMENTS

I would like to thank the Almighty God, the creator of heaven and earth for His guidance and protection towards me and my family.

Secondly, I would like to express my deepest gratitude to my supervisor, Dr Stephen Yamoah for his brilliant supervision, caring and providing an excellent atmosphere for doing this research. His continuous support and guidance helped me all the time in carrying out my research and writing of this thesis.

I also would like to thank Emeritus Prof E.H.K Akaho for his fatherly advice he gave me throughout my stay in the University and also his assistance in guiding this work. His help in developing my knowledge in Nuclear Engineering could not be underestimated.

I would like to thank the lecturers of Nuclear Engineering Department for their patience, guidance, enthusiastic encouragement and useful critiques of this research work. They were always willing to help and give their best suggestions.

I would also like to thank my colleagues in the CFD group, particularly Kafui, and Sadique for their valuable technical advice and cooperation.

A special thanks to my mother for her sacrifice she made on my behalf. At the end I would like to express my deepest appreciation to my beloved wife Beatrice Owusu-Manu, for her continuous support and encouragement.

TABLE OF CONTENTS **PAGE**

LIST OF TABLES

LIST OF FIGURES

LIST OF ABBREVIATIONS

RANS	Reynolds Average Navier-Stokes
SST	Shear Stress Transport
CFD	Computational Fluid Dynamics
MUSIG	MULtiple Size Group
HEM	Homogeneous Equilibrium model
CM	Class Methods
IAC	Interfacial area concentration
PBE	Population Balance Equation
CEL	CFX Expression Language
PBM	Population Balance Model
HEM	Homogenous equilibrium model
BWRs	Boiling water reactors
MOM	Method of moment
ECCS	Emergency core cooling system
CHF	Critical Heat Flux

DNS	Direct Numerical Simulation

NOMENCLATURE

C_{WL}	Wall Lubrication coefficient
C_D	Drag coefficient
C_L	Lift coefficient
C_{TD}	Turbulence dispersion coefficient
d_H	Maximum bubble horizontal dimension
d_n	Distance to the nearest surface
D_s	Bubble Sauter mean diameter
D_B, D_C	Mass birth rate due to break-up and coalescence
E_{cr}	Critical Heat flux
E_o	*Eötvös* number
$E_{O_{dg}}$	Modified *Eötvöv* number
f	Bubble size distribution
F_B	Break-up calibration factor
F_C	Coalescence calibration factor
F_{gl}^{WL}	Wall Lubrication Force for gas and liquid phase
$F_{\lg}^{WL}$	Wall Lubrication Force for liquid and gas phase
$F_{i,k}$	Total interfacial force
$F_{\lg}^{D}$	Drag force
$F_{\lg}^{L}$	Lift force

$F_{\lg}^{WL}$	Wall lubrication force
$F_{\lg}^{TD}$	Turbulent dispersion force
$f_{(i)}$	Size fraction
k	Turbulent kinetic energy
n	Average number density of gas phase
$\vec{n}_w$	Velocity vector
Pr_{tg}	Turbulent Prandtl number of the gas phase
R_b	Bubble radius
Re	Reynolds number
$S_{(i)}$	Mass transfer rate due to coalescence and break-up
t	Physical time
$\vec{u}_g$	Velocity vector for gas phase
$\vec{u}_l$	Velocity vector for liquid phase
U	Bubble terminal
U_t	Terminal velocity
V	Volume of bubble
y_w	Distance from the wall boundary
z	Volume fraction correction exponent

Greek symbols

α_l	Volume fraction of liquid Phase

μ_t	Turbulence viscosity
μ_{ts}	Shear induced turbulent viscosity
μ_l	Viscosity of the liquid
ρ	Density
ε	Turbulence eddy dissipation
ω	Weight
ξ	Weighted abscissas
α	Gas volume fraction
$\alpha_{\max}$	Maximum gas volume fraction
σ	Surface tension
ψ	Coalescence frequency
Γ	Collision frequency
λ	Coalescence efficiency
φ	Shear rate
Φ_{RC}	Bubble coalescence from random collisions
Φ_{WE}	Bubble coalescence from wake entrainment process
Φ_{TI}	Bubble breakup caused by impact of turbulent eddies

Subscripts

g	Gas phase
l	Liquid phase
gl	Transfer of quantities from gas to liquid phase
lg	Transfer of quantity from liquid to gas phase

i	Bubble size class
j	Velocity group

ABSTRACT

Gas–liquid bubbly flows are commonly encountered in many industrial processes. In many cases, the evolution of bubble size distribution is a crucial factor governing the momentum, heat and mass transfer between phases within the system. In this thesis, numerical investigation of gas-liquid bubbly flows is achieved by coupling a population balance model with the three-dimensional, two-fluid model. With the aim of evaluating the capabilities of the population balance model, a model validation study to assess the MUSIG model in a highly asymmetrical distributed bubbly flow in vertical pipe has been presented. Particularly, the research focus has been centered on detailed numerical investigation of the coalescence and breakup phenomenon by performing extensive numerical investigations for the examination and comparison of different model formulations. Two major contributions has been achieved in this thesis; (1) a modification of the coalescence model of Prince and Blanch (1990) to account for the imbalance between coalescence and breakup phenomenon; and (2) the population balance approach with implementation of the modified model into ANSYS CFX code using CFX Expression Language (CEL). Model predictions were validated against experimental measurements reported by Monros et al., (2013). Three different modifications (cases) have been investigated. Overall, predictions of the three cases were in satisfactory agreement with the experimental data. The transition from “wall peak” to “core peak” gas volume fraction profiles has been successfully captured. Encouraging results clearly demonstrates the applicability of the models for large scale industrial systems. In general, the comparison shows that the model labelled as Case 2 presented the best results in most of the experimental conditions.

Chapter 1

Introduction

The purpose of this Chapter is to present a description of the research work starting with introduction of background. Multiphase flow and the concept of gas liquid two phase flow with emphasis on bubbly flow have been explained. A brief description of the two main approaches in numerical simulation of gas-liquid bubbly flow and also the numerical models for solving them has been presented in this Chapter. The aims and objectives of the study are clearly presented and finally an outline of the overall thesis is provided at the end of this Chapter.

1.1 Background

Multiphase flow has extensively existed in academic researches and plays an important role in various industrial applications including power generation, energy conversion, and safety technology in power plants, paper manufacturing, and food processing as well as nuclear applications. Thus, a better understanding of multiphase flow interactions can lead to increases in performance, reduction in cost and improved safety in several important engineering desciplines (Sundaresan, 2000).

Up to very recently, the design of equipment involving multiphase flow relied strongly on correlations obtained experimentally. These experimental studies presented a number of difficulties: (1) the probes used for the measurement can interfere with the flow; (2) the multiphase system can be optically opaque; and (3) multiphase flows are well known for the difficulties in setting up fully controlled physical experiments. Fine measurements,

like the flow inside bubbles, or flows near the bubble surface to investigate the existence of local slip flow are not easy to realize.

Computer simulations, on the other hand, permit to include or neglect gravity, account for the effects of the geometrical configuration, process modifications and to perform many other variations in the physical problem. The great complexity of scales of the phenomena of practical multiphase flows with different length and time scales interacting in a broad range is difficult to model mathematically. An example is the coalescence of drops or bubbles where the interfaces are free to deform and breakup. The forces in such systems are very complex, of different types and in the spatial-temporal domain, they are observed over a large range of length scales (Hanrantty et al., 2003). The complex nature of multiphase flow originates from the existence of multiple, deformable and moving interfaces and attendant significant discontinuities of fluid properties and complicated flow field near the interphase.

Multiphase flow can be defined as a simultaneous fluid flow consisting of two or more phases, such as gas, liquid or solid. These flows can be classified in different forms depending on the state of different phases. In a multiphase flow, two-phase flow is the most common class that includes gas-solid, liquid-solid, gas-liquid flows. The multiphase flow systems and their physical phenomena have very little in common. This is because the flow is considered as heterogeneous mixture of multiple fluids or phases, which are not homogeneously mixed at a molecular level. Due to this fact, the tendency has been to analyze the problems of a particular system, component or process and develop systems specific models and corrections of limited generality and application. In addition, a broad understanding of thermo-fluid dynamics of two-phase flow has been only slowly

developed and, therefore, the predictive capability has not attained the level available for single-phase flow analysis.

The design of engineering systems and ability to predict their performance depend upon both the availability of experimental data and of conceptual mathematical models that can be used to describe the physical processes with a required degree of accuracy. Thus, it is essential that the various characteristics and physics of two-phase flow should be modelled and formulated on a rational basis and supported by detailed scientific experiments. This thesis work is focused on gas-liquid two-phase flow.

Gas-liquid two-phase flow is not only crucial to many industrial problems but also important in some natural processes, as in the ocean-atmosphere interactions. Typical gas-liquid two-phase flow problems consist of void and pressure wave propagation, bubble-driven circulation systems, as well as some well-known thermal-hydraulic and safety problems in nuclear reactor systems. In case of nuclear reactor systems, relevant issues include critical heat flux (CHF) problems, direct contact condensation from emergency core cooling system (ECCS) injection, flow oscillations in boiling water reactors (BWRs), and heat transfer through boiling. Gas-liquid two phase flows are considered the most complex due mainly to the fact that they combine a deformable interface and the compressibility of the gaseous phase (Hewitt, 2008). The dynamics of these flows is inherently complex as it is mainly influenced by the geometrical configuration in which the two phases are distributed. As these configuration depends mainly on the particle size (either bubbles or droplets), an in-depth phenomenological understanding of the processes that determine particle sizes and their dispersion is of paramount importance.

Gas-liquid two-phase flows can take different configuration. In this type of flow, either bubbles can travel in liquid flow or liquid droplets can travel in gas flow. In the first case, the liquid is considered as continuous phase and the bubble are assumed as disperse phase. For the second case, the gas is taken as continuous phase. When gas-liquid mixtures flow in a pipe, for example, they may distribute in variety of ways, which characterise the spatial distribution of mixtures within the pipe. In gas-liquid flow, the bubbles or droplets are moving and deformable in time and space domains and complex interactions occur between the interfaces, and also between the bubbles and the liquid flow. Since the bubbles or droplets are freely deformable within the continuous phase, they can form different geometrical shape, such as: spherical, taylor, and cap etc. The bubbly flow is normally observed where the gas is dispersed or suspended as small bubbles in the form of discrete particles in the liquid continuum. There exist complex interactions between the moving and deformable interfaces of bubbles, and also between bubbles and the liquid flow. The shape of the bubbles is typically nearly spherical and this is shown in Figure 1.1

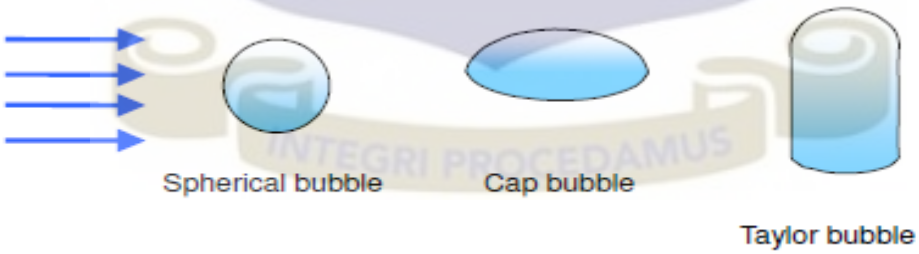

Figure 1.1 Bubble deformation (Lilunnahar et al., 2014)

Gas liquid two-phase flow can be classified according to the structure of interface into several major groups which can be called flow regimes or flow patterns such as separated

flow, transitional or mixed flow and dispersed flow, as shown in Table 1.1. Focusing on the dispersed flows and their subdivision by considering the phase of dispersion, we can distinguish three regimes: bubbly, droplet or mist, and particulate flow. This work is focused on gas-liquid two-phase bubbly flow. Table 1.1 summarises the various gas-liquid flow configurations (Ishii et al., 2006).

Table 1.1 Gas-Liquid two-phase flow classification (Ishii et al., 1976)

Flow transition	Flow regime	Configuration	Geometry
Dispersed flows	Bubbly	Gas bubbles in liquid	
	Droplet	Liquid droplets in liquid	
Mixed or transitional flows	Cap, Slug or Churn turbulent flows	Gas pocket in liquid	
	Bubbly annular	Gas bubbles in liquid film with gas core	
	Droplet annular	Gas core with droplets and liquid film	
	Bubbly droplet annular	Gas core with droplets and liquid film with gas bubbles	
Separated flows	Film	Liquid film in gas, gas film in liquid	
	Annular	Liquid core and gas film, gas core and liquid film	

Considering experimental visualization in gas-liquid two phase flow in vertical configuration, some commonly observed flow structures have been identified and classified, which have been depicted in Figure 1.2

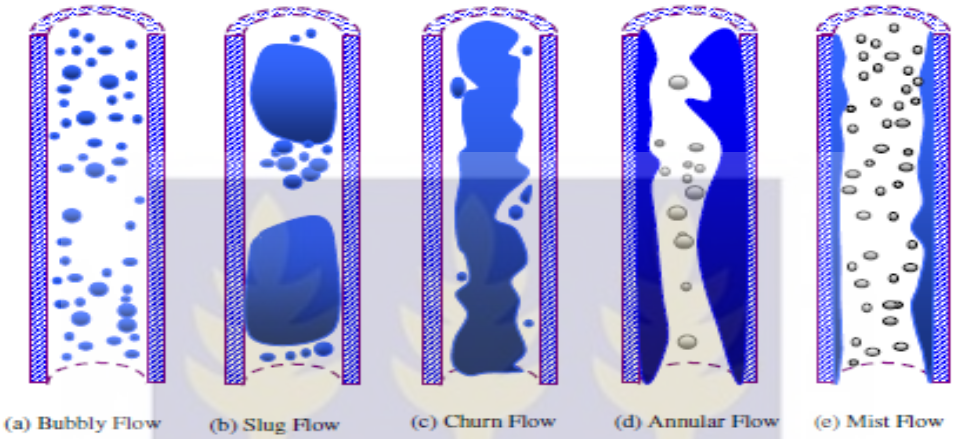

Figure 1.2 Flow patterns of air-water two-phase flow in vertical pipe (Li Cong et al., 2011)

The description of slug flow arise when the distance between bubbles decreases and the void fraction increases resulting in the bubbles colliding and coalescing together to form larger bubbles. These bubbles have hemispherical nose with a blunt tail end which usually flow up the pipe separated from one another by slug or liquid and surrounded by a thin film of liquid between them and the tube wall. These bubbles are called Taylor bubbles and in most cases they flow downward due to gravity force, although the fluid might flow upward. Figure 1.1 demonstrates the bubble deformation from spherical to cap and finally to Taylor bubble.

The churn flow pattern lies between slug and annular flow. Both slug and churn flow pattern show large fluctuations in void fraction and pressure drop. The behavior of churn flow is the to and fro motion of fluid with increasing velocity of flow, as a result the

structure of the fluid becomes unstable. This instability result from the gravity and shear stress on the thin film of the liquid of Taylor bubbles acting in opposite direction.

In Annular type of flow when the interfacial shear of high velocity gas on the liquid film becomes dominant over gravity force, the liquid is expelled from the center of the tube and flows as a thin phase up the center of the tube. Liquid may be carried in gas core as small droplets. Figure 1.3 shows a flow regime map that helps to identify the boundaries of possible flow region. The flow regime map is formed based on column diameter and the superficial gas velocity. The map described in Figure 1.3 is valid for both bubble and slurry bubble column. The transition between various flow regimes is indicated by the shaded area.

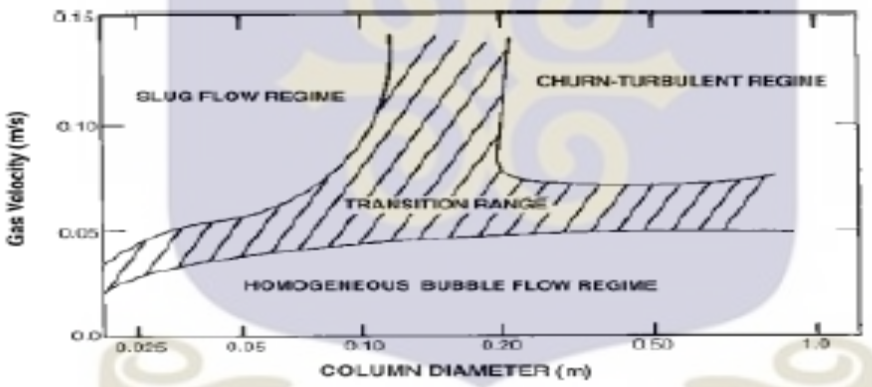

Figure 1.3 Flow regime map for bubble columns (Deckwer et al., 1980)

To find out the exact boundaries for transition from region to region, the individual systems need to be studied.

The increase in computational power and advancement of commercial modelling software have over the last decade resulted in an increasing number of studies on the

modelling of multiphase flow using computational fluid dynamics (CFD) approach. Computational fluid dynamics (CFD) is a computer-based tool for simulating the behaviour of systems involving fluid flow, heat transfer, and other related physical processes. It works by solving the equations of fluid flow over a region of interest, with specified (known) conditions on the boundary of that region. CFD has an advantage of showing detailed information in space and time (Alexopoulos et al., 2002), less empirical input (Harris et al., 1996), no scaling effects (Tatterson et al., 1994), can simulate tests that cannot be done in laboratories (Trambouze et al., 1993).

With increasing prevalence, the application of computational models has gained significant grounds in modelling multi-phase flows, such as dispersed gas-liquid flow or bubbly flow. There are two main approaches used in the numerical simulation of gas-liquid bubbly two-phase flow namely; Eulerian lagrangian and Eulerian-Eulerian models.

In the Eulerian-Lagrangian modelling, the continuous phase is solved by Euler framework solving the Navier-Stocks equations in the computational domain discretised into computational cells. The dispersed phase is simulated considering particles affected by forces from the continuous phase, and applying these forces on each particle. Within the Eulerian-Lagrangian model, the total flow of the particle phase is modelled by tracking a small number of particles through the continuous phase. The particles could be solid particles, drops or bubbles. The application of lagrangian tracking in CFX involves the integration of particle paths through the discretised domain. The solid particles, drops or bubbles is injected, in turn, to obtain an average of all particle tracks and to generate source terms to the fluid mass, momentum and energy equations.

The Eulerian-Eulerian model can be used to model any type of two-phase flow where the dispersed and the continuous phase are regarded as two interpenetrating phases. This model is the most generally adopted methodology to simulate multiphase flows (Venneker et al., 2002, Simom et al. 2000, Lehr et al. 2002). There are three main approaches used for the modelling of two-phase flow using the Eulerian-Eulerian formulation, i.e. the homogeneous equilibrium model (HEM), the drift flux model, and the separated or two-fluid model. The two fluid model is the most recommended and commonly used approach by investigators in order to solve bubbly flows (Bertodano et al., 1994, Trosnhko et al., 2002, Tillenkamp et al., 2002). The disperse phase entities such as the bubbles, particles and drops are assumed to be continuum just like the continuous phase. Each phase is governed by the Navier-Stokes equation. The phases interact with each other and share the same volume and as a result exchange mass, momentum and energy. Each phase is noted to have distinctive physical properties and in addition has its own velocity, pressure, concentrated and temperature field. Using empirical closure equations, the interphase transfer between phases is computed.

In the numerical study of bubbly two-phase flow, due to the existence of relative motion of one phase with respect to the other caused by differences of density and viscosity between the two phases, two separate velocity fields should be considered in any two-phase flow problem. Thus, in this thesis, the two-fluid model has been considered and investigated. For an isothermal bubbly flow without heat and energy transfer, the two-fluid model is simplified as only mass and momentum conservation equations of each phase with interfacial transport terms. The interfacial transports of mass and momentum usually have closely relationship to three important parameters (Ishii, 1975) viz: the

liquid turbulences, the interfacial driving forces and interfacial area concentration a_{if} (interfacial area per unit volume).

Turbulence consists of fluctuations in the flow field in time and space. It is a complex process, mainly because it is three dimensional, unsteady, consists of many scales and can have a significant effect on the characteristics of the flow. In principle, the Navier-Stokes equations describe both laminar and turbulent flows without the need for additional information. However, turbulent flows at realistic Reynolds numbers span a large range of turbulent length and time scales, and would generally involve length scales much smaller than the smallest finite volume mesh, which can be practically used in a numerical analysis. The Direct Numerical Simulation (DNS) of these flows would require computing power which is many orders of magnitude higher than available in the foreseeable future. Thus, to enable the effects of turbulence to be predicted, a large amount of CFD research has concentrated on methods that make use of turbulence models. These models have been specifically developed to account for the effects of turbulence without recourse to a prohibitively fine mesh and direct numerical simulation. The models generally seek to modify the original unsteady Navier-Stokes equations by the introduction of averaged and fluctuating quantities to produce the Reynolds Averaged Navier-Stokes (RANS) equations. The RANS equations represent the mean flow quantities only, while modelling turbulence effects without a need for the resolution of the turbulent fluctuations. Simulation of the RANS equations greatly reduces the computational effort compared to a Direct Numerical Simulation and is generally adopted for practical engineering calculations. The Shear Stress Transport turbulence model has been used in this thesis.

The interfacial force is an important closure term of the two-fluid model which represents the momentum transfer between these two individual phases. The interfacial driving force has been formulated through the interfacial transfer term of momentum conservation equation. The total interfacial force considered in this work is made up of drag, lift, wall lubrication and turbulence dispersion forces. It can be said that, among interfacial forces the drag force is the most important one since it represents the relative motions between two different phases and the relative motions are the fundamental information to calculate other interfacial forces.

The interfacial area concentration a_{if} which describes the available interfacial area per unit volume for the interfacial transport of mass, and momentum is very important parameter for efficiency of heat transfer and production of industrial facilities. Mathematically, the interfacial area concentration can be represented by the bubble number in certain spatial volume called bubble number density. For gas-liquid flows, the population balance model focuses on tracking the changes of bubbles number in finite space under the consideration of bubbles coalescence and breakup due to interaction among bubbles and between bubbles and turbulent eddies.

To account for the coalescence and breakup phenomenon of gas-liquid bubbly flows, the population balance modelling (PBM) has been used along with continuity and momentum equations within the two-fluid modelling framework.

The population balance model is made up of numerical approaches such as method of moments, Monte Carlo, and the Class Methods. Traditionally, population balance is implemented by using the class method (CM), in which a series number of discrete size

classes are utilized to approximate the continuous bubble size range. A more sophisticated model under the class method, namely the homogeneous MUSIG which was first introduced by Lo (1996), represents the most commonly used technique for solving PBM. The homogeneous MUSIG model assumes that all bubbles travel in one single velocity field. In this thesis, specific attention has been directed towards evaluating the performance of homogeneous MUSIG model in capturing the transition from wall peak to core peak in vertical pipe flow.

1.2 Aims and objectives

In two-phase flow conditions, the coalescence and breakup phenomena are happening simultaneously and both taking responsibility for the evolution of geometrical structure and bubble size distribution. However, the coalescence phenomenon is considered more complicated than breakup process. Since the coalescence and the breakup play significantly important roles of linking gas and liquid phases, the current study will look at optimizing and implementing the coalescence model of Prince and Blanch (1990) into ANSYS CFX. Two main objectives were completed in this thesis.

The first objective in this thesis is to present a model validation study to assess the MUSIG model in simulating flow conditions with wider range of bubble sizes in highly asymmetrical distributed bubbly flow in vertical configuration. Multiphase flow in bubbly flow regime shows a spectrum of different bubble sizes. At low volume fraction, the flow is homogeneous with mono-dispersed bubble size distribution. At high volume fraction, the flow regime becomes heterogeneous with broader bubble size distribution

resulting from coalescence and breakup phenomena. Thus accurate modelling of flow regimes should consider bubble coalescence and breakup phenomena.

The second objective of this work is to modify the coalescence model of Prince and Blanch (1990) by modelling additional expression to account for the coalescence calibration factor and implement this new model into ANSYS CFX. From literature, it has been observed that, experimentally the coalescence and breakup rates are not the same. For example Yamoah (2014) observed that the coalescence rate was about four times higher than the breakup rate in the experimental data used for his work. Similar observations in simulating bubble column flows have been reported. To correct this, calibration factors have been used to enhance the coalescence and breakup rates. Chen et al. (2005) enhanced the breakup rate by a factor of 10 in their numerical calculations. Olmos et al., (2001) used a calibration factor of 0.075 to enhance the breakup rates. Yamoah (2014) used a coalescence factor of $F_c = 0.05$ and break-up factor of $F_B = 0.2$ to enhance the coalescence and breakup rates. What this means is that, various researches must come out with their own calibration factors to match their experimental data and this is not representative enough. Since the experimental data used in this work is the same used by Yamoah (2014), the results of the new model have been compared with results from Yamoah (2014) for validation and verification of the new model. The gas volume fraction, interfacial area concentration, Sauter mean bubble diameter, liquid and gas velocities have been predicted for a wide range of gas and liquid flow conditions and validated with the experimental data reported by Monrós et al., (2013).

1.3 Outline of the thesis.

The contents of the thesis has been arranged into the following Chapters

Chapter 1 provides an introduction of the thesis beginning with an overview of multiphase flow with particular emphasis on gas-liquid two-phase bubbly flow. Also presented in this Chapter is a brief introduction of the two main approaches in numerical simulation of gas-liquid bubbly flow and the numerical models for solving them. This is followed by the objectives of the study.

Chapter 2 presents turbulence model based on Reynolds Averaging Navier Stokes equation and also modelling of turbulence in gas-liquid two-phase flow. The difference and the effects of $k-$ epsilon, $k-$omega and the shear stress transport models are clearly defined in this Chapter. The concept of the two-fluid model (that is the Eulerian-Eulerian) approach is dealt with in this Chapter. The detail analysis of the interfacial forces relevant for gas-liquid two-phase flow and the models used in this work are clearly explained. The Chapter also presents the population balance model and more emphasis was laid on the homogeneous MUSIG model for solving the PBEs. Finally, the Chapter concluded on the coalescence and breakup models used to solve the population balance equation.

Chapter 3 considered the methodology and this is divided into two parts. The first part has to do with the two-phase simulation methods which are implemented in the ANSYS CFX codes. Details of the computational domain, mesh sensitivity analysis, the boundary conditions, and numerical details have been presented. The second part considered the modelling of isothermal gas-liquid bubbly flow using the homogeneous MUSIG model

approach. Here, the sensitivity of size fraction distribution is presented and the set-up of calibration factor for coalescence in the MUSIG model and the breakup model are explained.

Chapter 4 presents the results and discussion of the numerical simulations. This Chapter is divided into two parts. The first part presents results obtained in this thesis. The second part presents a model verification study by comparing results from this thesis to that of Yamoah (2014)

Finally conclusion and recommendations are presented in Chapter 5. Further research work is also suggested.

Chapter 2

Literature Review

This Chapter is divided into four different Sections. First of all, the Chapter starts with description of turbulence modelling for two-phase flow. The second Section of this Chapter focuses on the two fluid modelling approach, where for isothermal bubbly flow conditions only the mass and momentum conservation equations were considered. The third Section considered the MUSIG model concept that have practical solution to the population balance equation and finally in Section four, the coalescence and breakup model for the homogenous MUSIG model is presented.

2.1 Turbulence modelling for two-fluid model

Turbulence modelling is of crucial importance for the correct description of multiphase flows in CFD modelling. For many years, turbulent phenomena has been a research interest and several authors have worked on this area and formulated models for multiphase flows (Jones and Launder, 1973; Kashiwa and VanderHeyden, 1998; Sokolichin and Eigenberger, 1999; Chahed et al., 2003).Whenever turbulence is present in certain flow it appears to be the dominant over all other flow phenomena. This explains why successful modelling of turbulence greatly increases the quality of numerical simulations. Turbulence, which consists of fluctuations in the flow field in time and space, generally exist in realistic flow conditions and significantly influence the characteristics of the flow. The Navier-Stokes equations in principle have the capability to solve both laminar and turbulent flows without the need for additional information (ANSYS CFX-14.5 User Manual). However, turbulence is a complex process involving

its three dimensions, unsteady and consists of many scales. By many scales, it means the turbulent flow span a large range of turbulent length and time scales, and would generally involve length scales much smaller than the smallest finite volume mesh. To account for the effects of turbulence without recourse to fine mesh, the statistical turbulence models are generally adopted for practical engineering calculations. These models with average and fluctuating quantities seek to modify the original unsteady Navier-Stokes equation to produce the Reynolds Averaged Navier-Stokes (RANS) equation. In the RANS approach for modelling turbulence, an approximation is introduced that all the flow unsteadiness is averaged out and the nonlinearity of the Navier-Stokes equations gives rise to terms that must be modelled. The method greatly reduces the computational effort, simple and possess good numerical stability. However it introduces additional unknown terms such as Reynolds stresses and Reynolds flux which need to be modelled by extra equations of known quantities in order to achieve closure (ANSYS CFX-14.5 User Manual).

The eddy viscosity model in which the Reynolds stresses are assumed to be proportional to mean velocity gradient is one of the most widely applied extra equations for Reynolds stresses and Reynolds flux. Thus, the searching of unknown terms Reynolds stresses and Reynolds flux is broken down to calculation of turbulence viscosity $\mu_{t,g}$.

Many turbulent models have been proposed to calculate the turbulence viscosity such as $k-\varepsilon$ model, $k-\omega$ model, their extensions Shear Stress Transport (SST) model.. In single-phase flow, the standard $k-\varepsilon$ model is generally used because of its simplicity and stability (Menter 1994). However in multi-phase flow, no standard turbulence model is suitable for all flow conditions. Cheung et al., (2007a) noted that the Shear Stress

Transport (SST) model developed by Menter (1994), was found superior to the standard $k-\varepsilon$ model . The SST model is a complex combination of the Wilcox models (Wilcos et al., 1988) to effectively blend the robust and accurate formulation of the $k-\omega$ model in the near-wall region with the free stream independence of the $k-\varepsilon$ model in the far field (Yamoah 2014) with a specific blending function. The SST model has been revealed to offer more practical prediction of gas volume fraction closer to the wall region of the flow domain. It avoids over prediction of the eddy-viscosity by accounting the transport of the turbulent shear stress and gives highly accurate predictions of the onset and the amount of flow separation under adverse pressure gradients. The SST model is employed in this thesis.

2.1.1 The Shear Stress Transport Model:

The transport equations of the SST model for bubbly flow can be expressed as:

$$\frac{\partial \rho_l \alpha_l k_l}{\partial t} + \nabla.(\rho_l \alpha_l \vec{u}_l k_l) = \nabla.(\alpha_l(\mu_l + \sigma_k \mu_{t,l})\nabla k_l) + \alpha_l P_{k,l} - 0.09\rho_l k_l \omega_l \qquad (2.1)$$

where

ρ_l is the density of liquid, α_l is the volume fraction of liquid phase, k_l is the turbulent kinetic energy of the liquid phase, μ_l is the viscosity of the liquid, ω is the weight, $\vec{u}_l$ velocity vector for liquid phase,

and

$$\frac{\partial \rho_l \alpha_l \omega_l}{\partial t} + \nabla.(\rho_l \alpha_l \vec{u}_l \omega_l) =$$
$$\nabla.(\alpha_l(\mu_l + \sigma_\omega \mu_{t,l})\nabla \omega_l) - 2\rho_l \alpha_l (1-F_1)\sigma_\omega \frac{1}{\omega_l}\frac{\partial k_l}{\partial x_j}\frac{\partial \omega_l}{\partial x_j} + \alpha_l \frac{\gamma}{v_t} p_{k,l} - \rho_l \beta \omega_l^2 \quad (2.2)$$

F_1 in equation (2.2) is a blending function defined such that close to the wall node the $k-\omega$ model is used and it changes to the $k-\varepsilon$ for the rest of the flow geometry

Let ϕ_1 represent any quantities in Wilcox model $(\sigma_{k1},.....)$ and ϕ_0 represent any constant in $k-\varepsilon$ model $(\sigma_{k0},.....)$ then $\phi = F_1\phi_1 + (1-F_1)\phi_0$ demonstrates the corresponding result of the new model $(\sigma_k,.....)$.

when $F_1 = 1$, $(k-\omega)$ is used: $\sigma_{k1} = 0.85$, $\sigma_{\omega 1} = 0.5$, $\beta_1 = 0.075$,

$$\gamma_1 = \beta_1/0.09 - \sigma_{\omega 1} k^2/0.3 \quad (2.3)$$

when $F_1 = 0$, the $k-\varepsilon$ model is used: $\sigma_{k0} = 1.0$, $\sigma_{\omega 0} = 0.856$, $\beta_0 = 0.0828$,

$$\gamma_1 = \beta_0/0.09 - \sigma_{\omega 0} k^2/0.3 \quad (2.4)$$

The shear induced turbulent viscosity μ_{ts} can be calculated from v_t such that:

$$\mu_{ts} = v_t \rho = \frac{0.31\rho k_l}{\max(0.31\omega_{l,} SF_2} \quad (2.5)$$

$$S = \sqrt{2S_{ij}S_{ij}} \quad (2.6)$$

where $S = \sqrt{2S_{ij}S_{ij}}$, is the absolute value of strain rate used in defining the eddy viscosity in the place of vorticity. This is done to raise the generality of the method above aerodynamic applications (Vieser et al., 2008). S is mass transfer rate due to coalescence and breakage

The success of SST model is mostly decided by the use of blending functions of F_1 and F_2 which is based on the distance to the nearest surface d_n and on the flow kinematic viscosity μ_t :

$$F_1 = \tanh\left(\theta_1^4\right) \tag{2.7}$$

$$\theta_1 = \min\left[\max\left(\frac{\sqrt{k_1}}{0.09\omega_l d_n}, \frac{500\mu_l}{\omega_l d_n^2}\right), \frac{4\rho_l k_l}{\max\left(\frac{2\rho_l}{\sigma_{\omega 2}\omega}\nabla k \nabla \omega, 10^{-10}\right)\sigma_{\omega o} d_n^2}\right] \tag{2.8}$$

$$F_2 = \tanh\left(\theta_2^2\right) \tag{2.9}$$

$$\theta_2 = \max\left(\frac{2\sqrt{k_l}}{0.09\omega_l d_n}, \frac{500\mu_l}{\omega_l d_n^2}\right) \tag{2.10}$$

Sato et al., (1981) argued that aside the effect of liquid phase shear induced turbulence which even happens in single phase flow, the existence of disperse phase in multiphase flow also contribute to turbulence in liquid phase. Thus, the dynamic viscosity of the liquid phase is modified to take into account the production and destruction of liquid turbulence due to agitation of bubbles. This effect can be accounted for using the Sato

bubble-induced turbulent viscosity model. The turbulent viscosity of liquid phase is therefore expressed as:

$$\mu_t = \mu_{ts} + \mu_{td} \tag{2.11}$$

$$\mu_{td,l} = C_{\mu p}\alpha_g D_s \left|\vec{u}_g - \vec{u}_l\right| \tag{2.12}$$

D_s *is the bubble diameter*

For the gas phase, the disperse phase zero equation model is utilized and the turbulent viscosity of the gas phase can thus be obtained as:

$$\mu_g^t = \frac{\rho_g}{\rho_l}\frac{\mu_t}{\mathrm{Pr}_{tg}} \tag{2.13}$$

where Pr_{tg} is the turbulent Prandtl number of the gas phase. Its value is set to unity. In two-fluid model, generally effective turbulent viscosity μ_{te} is required. It is subtotal of phase viscosity and turbulent viscosity.

2.2 The Two-Fluid Model

The two-fluid model can be considered as one of the most widely utilized method in bubbly flow due to its reasonable compromise between accuracy and computational cost. This model separately uses set of conservation equation to individually represent gas or liquid phase. For isothermal bubbly flow without mass and heat transfer as considered in this thesis, the three-dimensional two-fluid model conservation equation can be reduce to mass and momentum conservation equations.

Denoting the liquid as the continuous phase (α_l) and the gas bubbles phase as disperse phase (α_g), these equations can be written as:

The continuity equation for liquid phase:

$$\frac{\partial}{\partial t}(\rho_l \alpha_l) + \nabla(\rho_l \alpha_l \bar{u}_l) = 0 \tag{2.14}$$

Continuity equation for gas phase

$$\frac{\partial(\rho_g \alpha_g f_i)}{\partial t} + \Delta.(\rho_g u_g \alpha_g f_i) = S_i \tag{2.15}$$

where S_i is a source term due to coalescence and break-up, f_i is the bubble size distribution for a bubble size class.

Momentum equation of liquid phase

$$\frac{\partial}{\partial t}(\rho_l \alpha_l u_l) + .(\rho_l \alpha_l u_l u_l) = -\alpha_l \nabla P + \alpha_l \rho_l g + \nabla.\left[\alpha_l \mu_{e,l}\left(\nabla u_l + (\nabla u_l)^T\right)\right] + F_{\lg} \tag{2.16}$$

Momentum equation of gas phase

$$\frac{\partial}{\partial t}(\rho_g \alpha_g u_g) + \nabla.(\rho_g \alpha_g u_g u_g) = -\alpha_g \nabla P + \alpha_g \rho_g g + \nabla.\left[\alpha_g \mu_{e,g}\left(\nabla u_g + (\nabla u_g)^T\right)\right] + F_{gl} \tag{2.17}$$

where $\mu_{e,l}$ and $\mu_{e,g}$ are the effective viscosities of liquid and gas phases, respectively. The total interfacial force $F_{\lg}$ in equation (2.17) is formulated according to the appropriate consideration of different sub-forces affecting the interface between each phase

2.2.1 Interfacial momentum forces

The two-fluid model separately treats each of the phases with two set of conservation equations. Nonetheless, to close the conservation equation, it is required to provide the information on interfacial momentum transfer. The interfacial momentum force poseses significant influence on bubble size distribution in bubbly flow. Therefore, it is a crucial part in modelling gas-liquid flow. The total interfacial force consists of viscous drag force and the non-drag forces (such as, lift force, wall lubrication force and turbulence dispersion force). Neglecting the virtual mass force, the total interfacial force per unit volume for (k) is given as:

$$\vec{F}_{i,k} = \vec{F}_{\lg} = -\vec{F}_{gl} = \vec{F}_{\lg}^{D} + \vec{F}_{\lg}^{L} + \vec{F}_{\lg}^{WL} + \vec{F}_{\lg}^{TD} \tag{2.18}$$

Here, $\vec{F}_{\lg}$ denotes the momentum transfer terms from the gas phase to the liquid phase and vice versa for $\vec{F}_{gl}$. $\vec{F}_{\lg}^{D}$ is the momentum transfer due to drag force, $\vec{F}_{\lg}^{L}$ is the momentum transfer due to lift force, $\vec{F}_{\lg}^{WL}$ denotes the momentum transfer due to the wall lubrication force, $\vec{F}_{\lg}^{TD}$ is the momentum transfer due to turbulent dispersion force.

2.2.1.1 Drag force

The drag force represents the drag of one phase over the other. The origin of the drag force is due to resistance experienced by a bubble moving in liquid. The drag force consists of two parts of the form and the viscous drags. The form drag is caused by uneven pressure distribution around the moving bubble, and it is associated with bubble size and shape. The viscous drag is caused by the viscous stress related to fluid viscosity, and it is mainly produced within the boundary layer. Magnitudes of the form and the viscous drags vary with the bubble Reynolds number. When the bubble Reynolds number increases to a certain value, the flow begins to separate and form vortices behind bubbles, which results in an increase of the form drag. When the bubble Reynolds number is higher than a critical value, the viscous drag can be neglected, and the drag almost exactly comes from the form drag due to the start of the flow separation behind bubbles. As the bubble Reynolds number further increases, the drag coefficient nearly approaches a constant value, and the flow gradually transits to the inertial range. In the stokes flow region, the flow is thought of as a creeping flow in which the inertial terms in the Navier-Stokes equations are unimportant. With the bubble Reynolds number increasing, the inertial terms play more and more significant role in the bubble motion (Grevskott et al., 1996). Here, it should be pointed out that the flow separation behind bubbles is not same in the clean and contaminated liquid (Magnaudet et al., 2000). Whether the flow separation occurs or not depends strongly on the bubble shape and the mobility of interface. The drag coefficient is related to many factors. It was reported that the drag coefficient strongly depends on the bubble shape, orientation with respect to the flow as

well as on flow parameters such as the Reynolds number, *Eötvös* number, turbulent level, purity of bubble surface, and so on (Crowe et al., 1978; Takagi et al., 2008).

The interfacial momentum transfer between gas and liquid due to the drag force can be modelled as:

$$\vec{F}_{\lg}^{D} = \frac{1}{8} C_D a_{if} \left| \vec{u}_g - \vec{u}_l \right| (\vec{u}_g - \vec{u}_l) = -\vec{F}_{gl}^{D} \tag{2.19}$$

where a_{if} refers to the interfacial area concentration and C_D is the drag coefficient, which depends on the nature of the particles i.e., solid particles, drop or bubbles. The drag coefficient model based on the correlation of Grace et al., (1976) has been used in this thesis

2.2.1.1.1 Grace model

The Grace drag coefficient model (Grace et al., 1976) was first put originally together from a flow past a single distorted bubble, and was assumed to be applicable to sparse distribution fluid particles in the distorted regime. The Grace drag coefficient can be expressed as:

$$C_D = \frac{3}{4} \frac{gd}{U_t^2} \frac{\nabla \rho}{\rho_C} \tag{2.20}$$

where U_t is the bubble terminal velocity. From experiment, the terminal velocity was correlated as:

$$U_t = \frac{\mu_l}{\rho_l d_p} M_O^{-0.149}(J - 0.857) \tag{2.21}$$

To account for the case of densely distributed fluid particles, the model has been modified by using power law correction as expressed below (CFX-14.5, 2012)

$$C_D = C_{D\infty}\alpha_\alpha^P \tag{2.22}$$

where $C_{D\infty}$ is the single bubble drag coefficient as expressed in equation (2.20) and P is the volume fraction correction exponent depending on the bubble size.

Sometimes there are cases which need to be considered as totally diluted for example where there are groups of bubbles and they don't influence each other, it is possible to include a correction coefficient to account for the effect. When this happens, smaller bubbles will tend to move slower because of high void fraction and as a result the exponent becomes negative normally between 0 and -1. In the case of bigger bubbles, it will move faster at high void fraction and the exponent will be positive (CFX 14.5, 2012). From equation (2.20), U_t is the terminal velocity, given by:

$$U_t = \frac{\mu_C}{\rho_C d_b} M_O^{-0.149}(J - 0.857) \tag{2.23}$$

where M_O is the Morton number and J is a parameter defined as:

$$J = \begin{cases} 0.94H^{0.751} & 2 < H < 59.3 \\ 0.32H^{0.441} & H > 59.3 \end{cases} \tag{2.24}$$

In equation (2.23), H is expressed as:

$$H = \frac{4}{3} E_O M_O^{-0.149} \left(\frac{\mu_d}{\mu_{ref}} \right)^{-0.14} \tag{2.25}$$

μ_{ref} is the molecular viscosity of water and it is taken to be $0.0009 kg/ms$ (CFX-14.5, 2012).

The model is valid for $1.5 \times 10^{-12} < M_o < 10^{-3}$, $E_o < 40$ and $\mathrm{Re} > 0.1$ as recommended by Clift et al. (1978) for calculating the drag coefficient of droplets.

2.2.1.2 Lift force

The lift force accounts for the lateral force acting on the gas bubbles rising in a liquid. The lift force considers the interaction of the bubble with the shear field of the liquid. If the bubble moves within a non-uniform velocity field, the differences between the bubble velocities of the undisturbed liquid are asymmetrical, which cause an asymmetrical local pressure distribution at the bubble surface, hence, these results in a net lift force acting on the bubbles. The main components affecting the lift force (Hibiki 2007) are the relative velocity between the particle and its surroundings, the velocity gradient of the fluid around the particle, its own rotation, and its own surface if it can be considered slip or no-slip. In general the lift force per unit volume can be expressed for spherical bubbles as (Drew and Lahey 1987):

$$F_{\lg}^{L} = -F_{gl}^{L} = -C_L \alpha \rho_l \left(\vec{u}_g - \vec{u}_l\right) \times \vec{\omega} \tag{2.26}$$

The classical lift force for bubbles (Zun 1980), which has a positive coefficient C_L , acts in the direction of decreasing liquid velocity, i.e., in case of co-current upwards pipe flow in the direction towards the pipe wall. Numerical (Ervin et al., 1997; Schmidtke et al., 2005) and experimental (Tomiyama et al., 1995) investigations showed that, the direction of the lift force changes its sign, if a substantial deformation of bubble occur. The lift force has an important influence on the stability of bubble flows (Lucas et al., 2005c; 2006).

Tomiyama et al., (1995) performed both experimental and numerical investigations of the lateral migration of bubble in a laminar flow and quiescent liquid. They studied the effect of the *Eötvös* number and volumetric flux on the lateral motion of bubbles. They came up with some findings

1. Lateral force due to the wall region and a lift force due to circulation around the bubble away from the wall were found.
2. In quiescent liquid, they found that bubbles migrated to the center of the pipe and rose straight.
3. Increasing the liquid flux in either direction they found out that, it enhanced the lateral motion and that the lift force was proportional to the liquid flux.
4. They encountered negative values for lift force coefficient and this was due to the fact that, the bubble shape was distorted.

They concluded that, from the experimental data and numerical investigations, the lift force caused by the slanted wake, had the same functional form as that of the shear

induced lift force, and they proposed an empirical correlation of the lift coefficient which may change its sign depending on bubble deformation which results from the relation between gravitational force and surface tension force which must be based on *Eötvös* number.

There are other models for calculating the lift coefficient. The Magnaudet (1997) and Saffman (1965) are some models that have been used to solve the lift coefficient. In this thesis, the Tomiyama (1998) model for calculating the lift coefficient has been used since the model has the ability to account for the bubble deformation. However the model has been implemented with slight modification (Yamoah 2014).

Tomiyama (1998) studied single bubbles in a well-defined shear field and derived correlation for the coefficient of the lift force. The lift coefficient can be expressed as:

$$C_L = \begin{cases} \min\left[0.288\tanh\left(0.12\,\mathrm{Re}_g\right), f\left(Eo_{dg}\right)\right] & Eo_g < 4 \\ f\left(Eo_{dg}\right) = 0.00105Eo_{dg}^3 - 0.0159Eo_{dg}^2 - 0.0204Eo_{dg} + 0.474 & 4 \le Eo_g \le 10 \\ -0.29 & Eo_g > 10 \end{cases} \quad (2.27)$$

where the modified *Eötvös* number Eo_{dg} is defined as:

$$Eo_{dg} = \frac{g\left(\rho_l - \rho_g\right)d_H^2}{\sigma} \quad (2.28)$$

In equation (2.28), d_H is the maximum horizontal bubble diameter and can be expressed according to the correlation:

$$d_H = D\left(\frac{1}{E}\right)^{1/3} \tag{2.29}$$

where E is mean aspect ratio of the bubble.

To account for the aspect ratio of the bubble in equation (2.29), Tomiyama adopted the empirical correlation of Wellek et al., (1966) which can be expressed as:

$$E = \frac{1}{1+0.163E_O^{0.757}} \tag{2.30}$$

Yamoah (2014), Yamoah et al., (2015) noted that the correlation of Wellek et al. (1966) used for defining the maximum horizontal bubble diameter was obtained for liquid drops moving in stagnant liquid media and pointed out that drops and bubbles in purified systems are significantly more deformed than corresponding fluid particles in contaminated systems. The greatest effect of system purity being in the ellipsoidal regime, where small bubbles and drops being spherical have aspect ratio of one $(E=1)$ and for large or deformed bubbles the aspect ratio approaches a value of 0.24 $(E=0.24)$ (Yamoah, 2014).

Using dataset that was obtained after a set of measurements of air bubbles rising in stagnant water from Cai et al. (2010), Yamoah obtain a new correlation for the bubble aspect ratio as:

$$E_b = 0.5 + \frac{0.5}{1+(Eo-0.05)^{2.3}}\left(1+0.26Eo^{1.6}\right) \tag{2.31}$$

The dataset was taken for bubble Eötvös numbers between 0.3 and 10 (1.5 and 12 mm diameter) approximately, so it seems to be quite appropriate for the experimental conditions to be simulated in this thesis. Thus, in this thesis the correlation expressed in equation (2.31) is used instead of equation (2.30).

Hence the maximum horizontal bubble diameter using equation (2.29) can be expressed as:

$$d_H = D_b\left(2+\frac{1+(Eo-0.05)^{2.3}}{0.5\left(1+0.26Eo^{1.6}\right)}\right) \tag{2.32}$$

Yamoah et al. (2015) noted that the use of Cai's correlation instead of Wellek's does not change significantly the form of the lift force coefficient, that is given by equation (2.27), but the location of the sign reversal. It takes place around $D_b = 5.8mm$ with Wellek's correlation, and around 4.3 mm with the new correlation.

2.2.1.3 Wall lubrication Force

In contrast to the lift force, lateral force due to the surface tension is formed to prevent bubbles attaching on the solid walls thereby resulting in a low gas void fraction at the vicinity of the wall area. This force is well-known as wall lubrication force which can be modelled according to Antal et al. (1991) given by

$$F_{\lg}^{WL} = -F_{gl}^{WL} = -\left(C_{W1}+C_{W2}\frac{D_S}{y_w}\right)\frac{\alpha_g\rho_l\left[\left(\vec{u}_g-\vec{u}_l\right)\right]-\left(\left(\vec{u}_g-\vec{u}_l\right)\right)\vec{n}_w\vec{n}_w\Big]^2}{D_S} \tag{2.33}$$

where y_w is the distance from the wall boundary, $\vec{n}_w$ is the outward vector normal to the wall, and C_{w1}, C_{w2} are non-dimensional coefficients which have a default value in ANSYS CFX as $C_{w1} = -0.01$ and $C_{w2} = 0.05$ (Antal et al., 1991).

The implementation of the wall lubrication force is necessary as it reproduces the void peak near the wall for adiabatic two-phase flows. Lucas et al., (2004), Krepper et al., (2007) observed that, the use of wall lubrication force at high pressure wall boiling condition is not representative enough; therefore, it is proper to consider it in isothermal upward bubbly flow at atmospheric pressure and room temperature.

2.2.1.4 Turbulent dispersion force

Turbulent dispersion force came as a result of diffusion caused by turbulence and this force determines the sharpness of the wall peak. Again, in situations where we have a negative lift force coefficient, the turbulence dispersion force act to disperse the bubbles to the center. Burns et al., (2004) used the Favre-averaging to formulate an expression for the turbulent dispersion force as:

$$F_{\lg}^{TD} = C_{TD}\left[\frac{1}{8}C_D\alpha_{if}\rho_l\left|u_g - u_l\right|\right]\frac{\mu_g^t}{\rho_g Sc_b}\left(\frac{\nabla\alpha_g}{\alpha_g} - \frac{\nabla\alpha_l}{\alpha_l}\right) \tag{2.34}$$

where μ_g^t is the turbulent viscosity of the gas phase. Sc_b represents the bubble Schmidt number valued to 0.9.

2.2.1.4.1 Lopez de Bertodano Model

Another well-known model used for turbulent dispersion force is the Lopez de Bertodano model. The model of Lopez de Bertodano (1991) is expressed as:

$$F_{\mathrm{lg}}^{TD} = -F_{gl}^{TD} = -C_{TD}\rho_l e_l \nabla \alpha_g \tag{2.35}$$

e_l is the turbulent kinetic energy in the continuous phase. It was found by Lopez de Bertodano et al., 1994a, 1994b that the C_{TD} value of 0.1 to 0.5 gives good results for medium sized bubbles in the ellipsoidal particle regime. Again, according to Lopez de Bertodano, 1998; Moraga et al., 2003, smaller bubbles or solid particles were found to require very different value of C_{TD}, up to 500. The Lopez de Bertodano., (1991) model was improved to Lopez de Bertodano., (1998) and the new model is presented as:

$$C_{TD} = C_{\mu}^{1/4} \frac{1}{St(1+St)} \tag{2.36}$$

where $St = \frac{\tau_d}{\tau_c}$ is the stokes number, τ_d is the bubble response time and τ_c is the time response of the continuous phase in existence of the dispersed one (Moraga et al., 2003).

$$\tau_d = \frac{8}{3}\frac{R_b}{C_D|u_{rel}|} \tag{2.37}$$

$$\tau_c = C_{\omega}^{1/4}\frac{k}{\varepsilon} \tag{2.38}$$

where C_ε = 0.09. R_b is the bubble radius, k is the turbulent kinetic energy of the continuous phase and ε is the turbulent dissipation rate.

2.3 POPULATION BALANCE MODELLING

The evolution of the population balance model has a long standing history. At the end of 18th century, the Boltzmann equation, devised by Ludwig Boltzmann, could be regarded as the first population balance equation which can be expressed in terms of statistical distribution of molecules or particles in a state space. Nonetheless, the derivation of a generic population balance concept was actually initiated from the middle of 19th century. In 1960s, Hulburt and Katz (1964) and Pandolph and Larson (1964), based on the statistical mechanics and continuum mechanical framework respectively, presented the population balance concept to solve particle size variation due to nucleation, growth and agglomeration processes. Thereafter, a series of research development have been presented (Fredrickson et al., 1967; Ramkrishna 1979, 1985) where the treatments of population balance equations (PBE) were successfully generalized with various internal coordinates. The flexibility and capability of population balance in solving practical engineering problems has not been fully exposed, until recently, where Ramkrishna (2000) wrote a text-book focusing on the generic issues of population balance for various applications such as liquid-liquid extraction, gas-liquid dispersions, liquid-liquid reactions. Owing to the complex phenomenological nature of particle dynamics, analytical solutions has only existed in very few cases of which coalescence and breakup kernels are substantially simplified (Scott, 1968; McCoy and Madras, 2003).

Driving by practical interest, numerical approaches have been developed to solve the PBEs. The most common methods are Monte Carlo methods, Method of Moments and the Class Methods. The Monte Carlo methods, which solve the PBE based on statistical ensemble approach (Domilovskii et al., 1979; Liffman et al., 1992; Debry et al., 2003; Maisel et al., 2004), are attractive in contrast to other methods. The method is flexible and can accurately track particle changes in multidimensional systems. The accuracy of the Monte Carlo method is directly proportional to the number of simulations of the particles, thus, requiring extensive computational time. This makes the method very expensive. Furthermore, incorporating the method into conventional CFD program is also not straightforward which greatly degraded its applicability for industrial problems.

The method of moments (MOM) was first introduced by Hulburt and Katz (1964), and is considered as one of the promising approaches in attaining practical solutions to the PBE. The idea of the MOM centres in the transformation of the problem into lower-order of moments of the size distribution. The MOM has the advantage of tracking the evolution of limited number of moments (Frenklach, 2002) thus, requiring less computational time compared to the Monte Carlo method. This becomes a critical value in modeling complex industrial systems when particle dynamics is coupled with already time-consuming calculations of turbulence multiphase flows.

Traditionally, population balance is implemented by using the class Method (CM), in which a series number of discrete size classes are utilized to approximate the continuous bubble size range. The traditional class method has long standing history of development and straightforward implementation in many commercial CFD software packages. The method discretizes the particles into a series number of discrete size classes. For each

class, a scalar (number density of particles) equation is solved to accommodate the population changes caused by intra/inter-group particle coalescence and breakage. The interfacial area transport equation (IATE) and the multiple size group (MUSIG) methods are example of the class method. In this thesis, the MUSIG model has been adopted for the study of gas-liquid two-phase bubbly flow.

2.3.1 MUltiple Size Group (MUSIG) model

The MUSIG model has received increasing attention and is being gradually adopted as the preferred method for population balance modelling. It provides a convenient framework so that the population balance method can be incorporated into three-dimensional CFD calculations. The model has been developed to handle poly-dispersed multiphase flow. By poly-dispersed multiphase flow, it means that the dispersed phase has a large variation in size. In the MUSIG model, the continuous particle size distribution (PSD) function is approximated by M number size fractions; the mass conversation of each size fractions are balanced by the inter-fraction mass transfer due to the mechanisms of particle coalescence/agglomeration and breakage processes. The overall PSD evolution can then be explicitly resolved via source terms within the transport equations.

For larger gas volume fractions, several bubble size classes have to be considered and the exchange of mass between them caused by bubble coalescence and breakup phenomena has to be taken into account. In principle, the Eulerian-Eulerian two-fluid approach as described above (Section 2.2) can be extended to simulate a continuous liquid phase and several gaseous dispersed phases solving the complete set of balance equations for each phase. The investigations however showed that for an adequate description of the gas

volume fraction profile including a population balance model decades of bubble size classes would be necessary. In a CFD code, such a procedure is limited by the increased computational effort to obtain converged flow solutions. To solve this problem, the MUSIG model has been developed to account for different bubble shapes (sizes) and travelling dispersed phase velocities. By describing the spectrum of bubble size through a series of discrete bubble size classes, the dynamical changes of the size distribution can be tracked. Depending on assumption of same or different velocities in same size group, the MUSIG model has been classified as homogeneous or inhomogeneous MUSIG model as depicted in Figure 2.1.

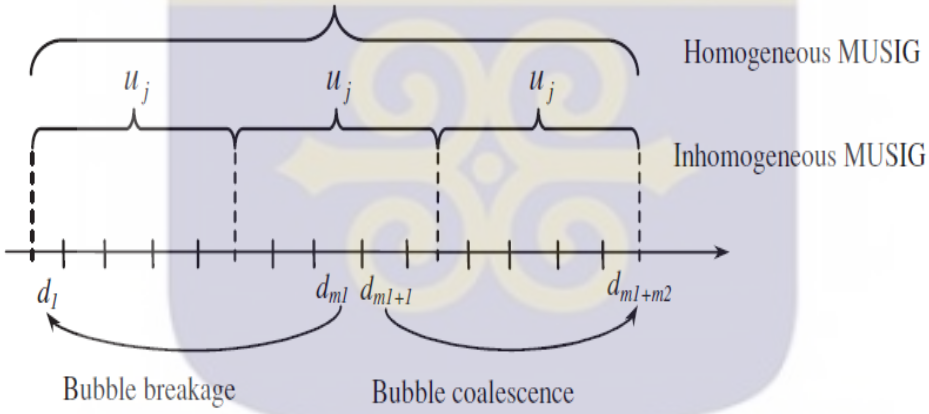

Figure 2.1 Schematic diagram of the homogeneous and inhomogeneous models (Cheung 2009)

The homogeneous MUSIG model solves one common momentum equation for all bubble size classes (Lo 1996). The model is based on the population balance method and the two-fluid modelling approach. The dispersed phase is divided into M size fractions. The population balance equation is applied to describe the mass conservation of the size fractions taking into account of the inter-fraction mass transfer resulting from bubble

coalescence and breakup. This model approach allows a sufficient number of size fraction groups required for the coalescence and breakup calculation to be used and has found a number of successful applications to large-scale industrial multiphase flow problems.

In the inhomogeneous MUSIG model (Krepper et al., 2005), the gaseous disperse phase is divided into a number M of so-called velocity groups (or phases), where each of the velocity groups is characterized by its own velocity field. Also, the overall bubble size distribution is represented by dividing the bubble diameter range within each of the velocity group's j into a number of sub-size fractions. The population balance model considering bubble coalescence or bubble breakup is applied to the sub-size groups. Thus, the mass exchange between the sub-size groups can exceed the size ranges assigned to the velocity groups resulting in mass transfer terms between the different phases or velocity groups.

The formulation of the MUSIG model originates from the discretized population balance equation given by:

$$\frac{\partial n_i}{\partial t} + \nabla.\left(n_i \vec{u}\right) = \sum_j R_j \qquad (2.39)$$

$\sum_j R_j$ denotes the source term as in equation 2.39

Equation 2.39 can be re-expressed in terms of size fraction f_i of M bubble size groups according to (Kumar and Ramkrishna, 1996a, b). This is to make sure that the overall

mass conservation for poly-dispersed vapour phase is captured correctly. The equation is therefore expressed as follows:

$$\frac{\partial(\rho_g \alpha_g f_i)}{\partial t} + \Delta.(\rho_g u_g \alpha_g f_i) = S_i \tag{2.40}$$

with

$$\alpha_g = \sum_{j=1}^{M} \alpha_j \tag{2.41}$$

$$\alpha_g + \alpha_l = 1 \tag{2.42}$$

$$\sum_{j=1}^{M_j} f_i = 1 \tag{2.43}$$

S_i is responsible for: the birth of bubbles of size i due to breakup of larger size and coalescence of bubbles of smaller size, B_{bi}, B_{ci}; and also the death of the bubbles of size i due to both break up and coalescence encountered in this size group, D_{bi}, D_{ci}. The source term S_i can thus be expressed as:

$$S_i = B_{bi} - D_{bi} + B_{ci} - D_{ci} \tag{2.44}$$

B_{bi} can be expressed as follows:

$$B_{bi} = \rho_j \alpha_j \left(\sum_{j>i} \Omega(m_j, m_i) f_j \right) \tag{2.45}$$

The death rate due to breakup can be expressed as:

$$D_{bi} = \rho_j \alpha_j \left(f_i \sum \Omega(m_j, m_i \right) \tag{2.46}$$

The birth rate due to coalescence is given by:

$$B_{ci} = \left(\rho_j \alpha_j\right)^2 \left(\frac{1}{2} \sum\sum \Gamma(m_j m_k \right) X_{iki} f_j f_k \frac{m_j + m_k}{m_j m_k} \tag{2.47}$$

The death rate due to coalescence is given as:

$$D_{ci} = \left(\rho_j \alpha_j\right)^2 \left(\sum \Gamma(m_i, m_j \right) f_i f_j \frac{1}{m_j} \tag{2.48}$$

X_{jki} denote the coalescence mass matrix which can be defined as the fraction of mass due to coalescence between groups j at t, which goes into group i, m_i is the mass fraction of the particular size group i, Ω and Γ are breakup and coalescence kernel function, respectively.

$$X_{jki} = \begin{cases} \dfrac{\left(m_j + m_k\right) - m_{i-1}}{m_i - m_{i-1}} & if \;\; m_{i-1} < m_j + m_k < m_i \\ \dfrac{m_{i+1} - \left(m_j + m_k\right)}{m_{i+1} - m_i} & if \;\; m_i < m_j + m_k < m_{i+1} \\ 0 & otherwise \end{cases} \tag{2.49}$$

2.4 MECHANISMS AND MODELS FOR BUBBLE COALESCENCE AND BREAKUP

2.4.1 Bubble Interaction Mechanisms

The interfacial area concentration is a key parameter that links the interaction between the gas and liquid phases for the study of transient multiphase flows. Apart from breakup and mass transfer, coalescence is responsible for the evolution of bubble sizes in multiphase flows. Thus, the study of fluid particle dynamics (coalescence and breakup) has become relevant due to many industrial applications involving multiphase flow.

To demonstrate the mechanisms responsible for bubbles coalescence and breakup, Wu et al., (1998) classified the processes as follows Figure 2.2:

- Coalescence through random collision driven by turbulent eddies
- Coalescence due to the acceleration of the following bubble in the wake of the preceding bubble
- Break-up due to the impact of turbulent eddies
- shearing-off of small bubbles from larger cap bubbles
- breakup of large cap bubbles due to interfacial instabilities

For bubbly flow conditions where no cap bubbles are present as considered in this thesis, the first three major phenomenological mechanisms are considered.

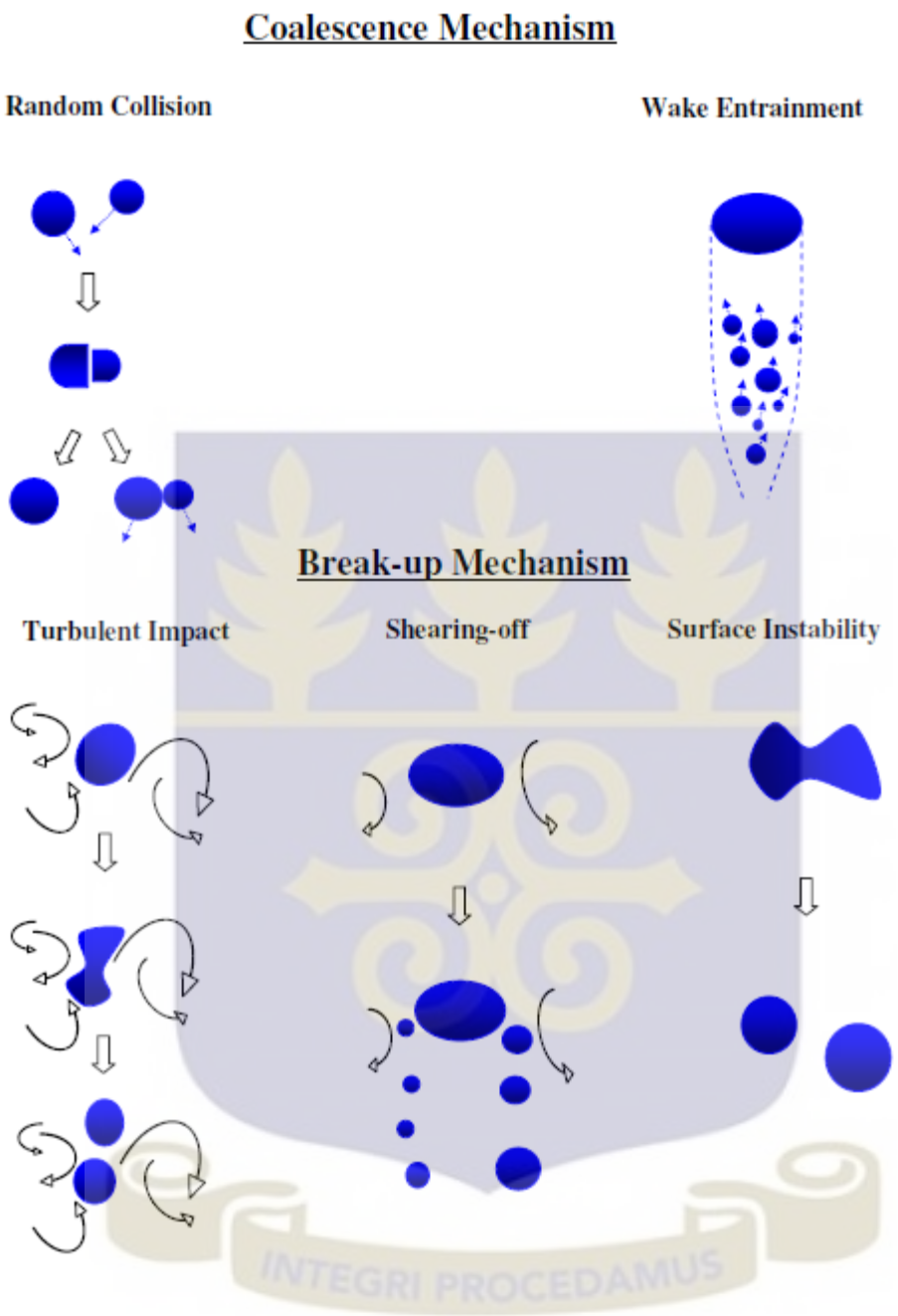

Figure 2.2: The Schematic Illustration of Bubble Coalescence and Break-up Mechanisms (Cong Li, 2012)

2.4.1.1 Mechanisms of fluid particle coalescence

Coalescence is considered more complex as compared to breakup (Chesters 1991) because it involves not only the interactions of bubbles with surrounding liquid, but also

those between bubbles themselves once they are brought together by the external flow or by body forces. Three theories or criteria have been proposed in literature for the coalescent process. The most popular theory is the film drainage model proposed by shinnar and church (1960). According to this model, the coalescence process can be divided into three manageable sub processes: (1) two bubbles collide, trapping a small amount of liquid between them; (2) bubbles keep in contact till the liquid film drains out to the critical thickness; (3) the film raptures resulting in coalescence. On the other hand Howarth (1994) argues that the attraction force between two colliding interfaces, usually of molecular nature is too weak in comparison with the turbulent force to control the coalescence probability., Thus for coalescence to occur will depends on the impact of the colliding bubbles. In more recent work, Lehr et al. (2002), Lehr and Mewes (1999) introduced the critical approach velocity model, which is an empirical theory based on the experimental observation of Doubliez, (1991) and Duinevald, (1994) that small approach velocities lead to high coalescence efficiency.

Among all the theories, contact and collision is the premise of coalescence. The collision between bubbles is usually caused by their relative velocity. However, not all collision lead to coalescence and most of them bounce back from each other after collision. Therefore, the concept of efficiency or probability is introduced. The coalescence frequency is thus determined by both collision frequency $h(u-u_1,u_1)$ and coalescence efficiency $\lambda(u-u_1,u_1)$. That is

$$\Psi(d_i,d_j)=h(d_i,d_j)\lambda(d_i\,d_j) \tag{2.50}$$

In Figure 2.3, the main theories and models for the coalescence frequency are classified.

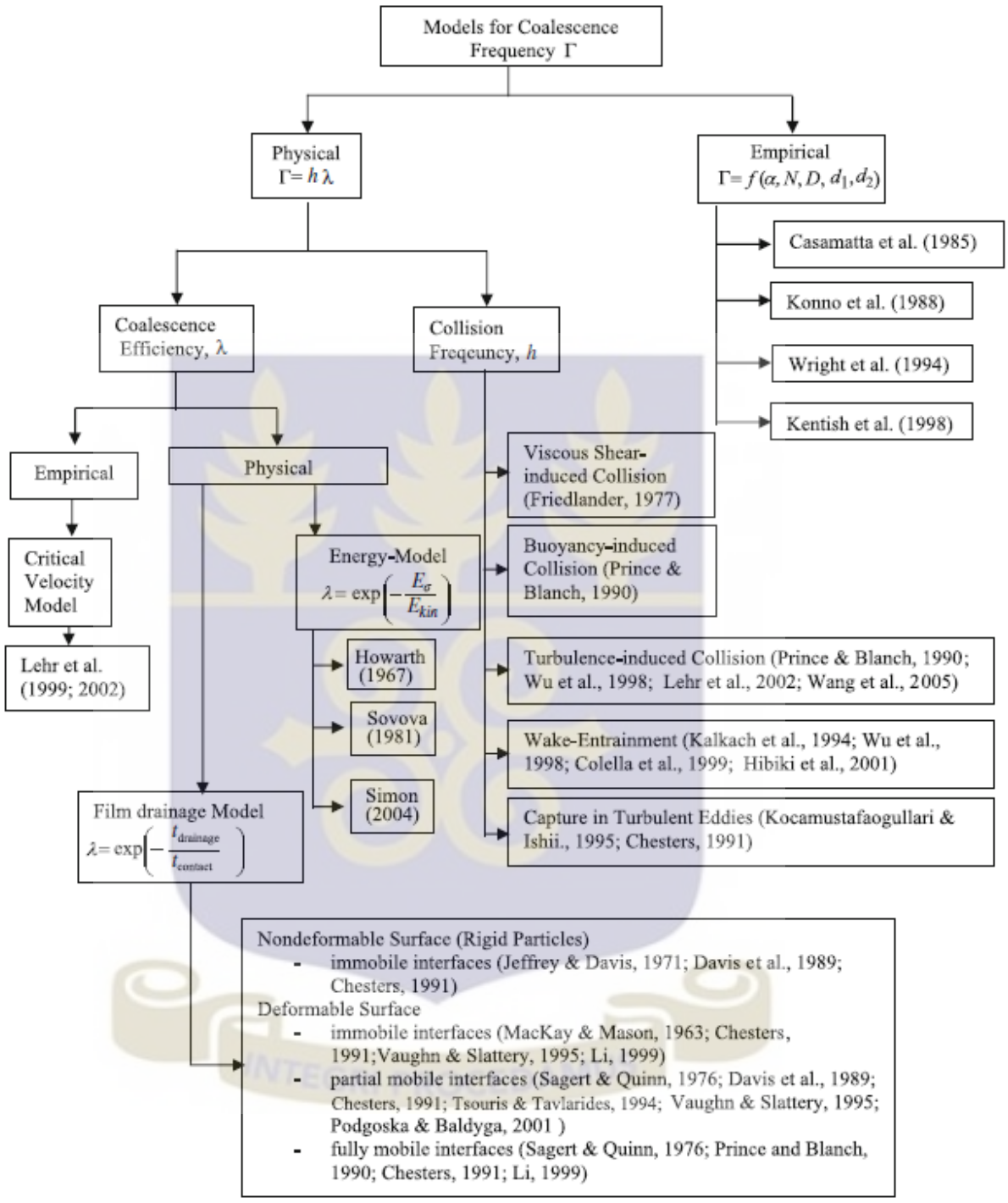

Figure 2.3: Classification of coalescence efficiency models (Liao and Lucas. 2010).

2.4.1.2 Collision Frequency

For a turbulent bubble flow, the relative motion that causes collision between bubbles may occur due to a variety of mechanisms. These include; motion induced by turbulent fluctuations in the surrounding continuous phase, motion induced by mean velocity gradients in the flow, different bubble rise velocities induced by buoyancy or body forces, bubble capture in an eddy, wake interactions or helical/zigzag trajectories. It is clear that collisions may result from the random motion of bubbles due to turbulent fluctuations and in addition bubbles located in region of relative high liquid velocity may collide with bubbles in a slower velocity field. Furthermore, if two bubbles are simultaneously captured in one eddy, they may coalesce with each other due to the shear rate of the flow in the eddy. Finally, because of body forces (buoyancy) and wake interactions, bubbles of different sizes will have different rise velocities and may collide with each other.

In a turbulent bubbly flow as considered in this thesis, collision resulting from the fluctuating turbulent velocity of the surrounding liquid is considered as the most dominating factor.

In a turbulent flow, the random motion of fluid particles is usually assumed to be similar to the random movement of gas molecules in the classical kinetic gas theory. Thus, under the assumption of random movement similarity between gas molecules and fluid particles, the collision frequency can be expressed based on the classical kinetic theory of Kennard (1938) as:

$$\Gamma_{turb}(d_i, d_j) = S_{ij} u_{rel} \tag{2.51}$$

Where d_i, d_2 is two different bubble size and the cross-sectional area of the two colliding bubbles, S_{ij}, is calculated as:

$$S_{ij} = \frac{\pi}{4}(d_i + d_j)^2 \tag{2.52}$$

In order to determine the approach velocity u_{rel} it is usually assumed that the colliding bubbles take the velocity of an equal-size eddy (coulaloglou and Tavlarides, 1977; Lee et al., 1987; Prince and Blanch, 1990; Luo, 1993). It must be noted that a small eddy does not contain sufficient energy to affect bubble motion and that much larger eddies transport only bubbles and have no effect on the relative motion. Consequently, the relative velocity between two bubbles of size d_i and d_j is proportional to the mean-square root of two equivalent eddy-velocities.

$$u_{rel} = \left(u_{ti}^2 + u_{tj}^2\right)^{1/2} \tag{2.53}$$

Where u_{ti} is the velocity of eddy with size, d_i

Applying classical turbulent theories, the eddy velocity u_t can be determined assuming inertial subrange of isotropic turbulence so that:

$$u_t^2 = C_{13}(\varepsilon d)^{2/3} \tag{2.54}$$

Finally, the collision frequency can be expressed as (Lee et al., 1987; Luo, 1993)

$$h(d_i, d_j) = C_{14}\frac{\pi}{4}(d_i + d_j)^2(d_i^{2/3} + d_j^{2/3})^{1/2}\varepsilon^{1/3} \tag{2.55}$$

Although equation (2.43) is widely used for the calculation of collision frequency, some modification factors have been proposed in more recent work. The first modification factor accounts for the effect of size ratio between bubbles and eddies.

According to Colin et. al., (2004), turbulent eddies are not efficient to move the bubbles and that the relative bubble motion is mainly due to the mean shear of the flow if the bubbles are larger than the integral length scale of turbulence l_e. Therefore, turbulence-induced collision may occur only in the following cases:

Case1: $(D_i \prec l_e; D_j \prec l_e),\ u_{rel} = \frac{C_t}{\sqrt{1.61}}\left(\varepsilon \frac{D_i + D_j}{2}\right)^{1/3}$ (2.56)

Case 2: $(D_i \prec l_e; D_j \succ l_e),\ u_{rel} = \frac{C_t}{\sqrt{1.61}}(\varepsilon D_i)^{1/3}$ (2.57)

where the coefficient, C_t, takes into account the difference between the velocity of bubbles and the eddies, which has been neglected previously, while the factor $1/\sqrt{1.61}$ considers the deceleration of the approaching bubbles due to an increase in their mass.

The second modification is to consider the existence of bubbles that reduces the free space for bubble movement and causes an increase in the collision frequency. The effect can be described by multiplying the collision frequency with factor, γ. Different expressions of factor γ can be found in literature and summarized in Table 2.1

Table 2.1 Different Expressions for Factor γ (Liao et al., 2010).

Reference	Factor γ	α max [a]
Wu et al. (1998)	$\frac{1}{\alpha_{max}^{1/3}(\alpha_{max}^{1/3}-\alpha^{1/3})}$	0.8
Hibiki and Ishii (2000a,2000b)	$\frac{1}{(\alpha_{max}-\alpha)}$	0.52(2000a) 0.741(2000b)
Lehr et al. (2002)	$\exp[-\left(\frac{\alpha_{max}^{1/3}-\alpha^{1/3}}{\alpha^{1/3}}\right)^2]$	0.6
Wang et al. (2005a,2005b)	$\frac{\alpha_{max}}{\alpha_{max}-\alpha}$	0.8

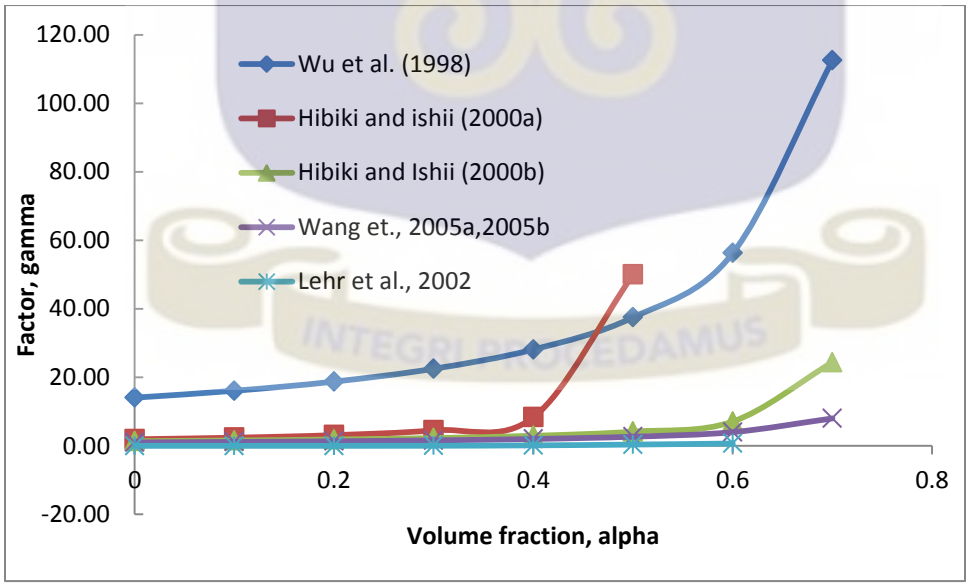

Figure 2.4 The dependency of factor γ on volume fraction α

Another modification one can notice in literature is about the ratio of the mean distance between bubbles to their average relative turbulent path length. Wu et al. (1998) and Wang et al. (2005a) suggested that when the distance between bubbles is larger than the turbulent path length, no collision should be counted, therefore a decreasing factor π should be added to equation 2.44

Wu et al. (1998) proposed the following modification factor:

$$\Pi = \left[1 - \exp\left(-C_{16}\frac{I_t}{h_{b,12}}\right)\right] \tag{2.58}$$

where I_t is the average size of eddies that drive bubble of size;

d_1, d_2.

By assuming the average size of eddies to be on the same order of the bubble size, the final form for the factor Π derived by Wu et al. (1998) for one group case is:

$$\Pi = \left[1 - \exp\left(-C\frac{\alpha_{\max}^{1/3}\alpha^{1/3}}{\alpha_{\max}^{1/3} - \alpha^{1/3}}\right)\right] \tag{2.59}$$

where C is an adjustable parameter, depending on the properties of the fluid, C=3 used by Wu et al. for the air-water system.

On the other hand, Wang et al. (2005a, b) employed a different correlation by considering that Π should approach unity when $h_{b,12}/l_{bt,12}$ is small and approach zero at large ratios so that:

$$\Pi = \exp\left[-\left(\frac{h_{b,ij}}{l_{bt,ij2}}\right)^6\right] \tag{2.60}$$

where the ratio of the mean distance between bubble size is d_1, d_2 and $l_{bt,ij2}$ is the mean relative turbulent path.

where $l_{bt,ij}$ is the mean relative turbulent path length scale of bubble with size d_1 and d_2 . Lehr et al. (2002) on the other hand assumed that the effective range of turbulent fluctuations obeys a normal distribution and proposed the following expression for the factor Π as:

$$\Pi = \exp\left[-\frac{\alpha_{\max}^{1/3} - \alpha_g^{1/3}}{\alpha_g^{1/3}}\right] \tag{2.61}$$

with $\alpha_{\max} = 0.6$.

Applying these calibration factors, the final form of the collision frequency can be expressed as:

$$\Gamma_T(D_i, D_j) = C\gamma\Pi\frac{\pi}{4}(D_i + +D_j)^2(D_i^{2/3} + D_j^{2/3})^{1/2}\varepsilon^{1/3} \tag{2.62}$$

Essentially, the calibration factors Π and γ play a similar role, both related to the volume fraction (α or number density of bubbles.

2.4.1.3 Coalescence Efficiency

A number of experiments have shown that most of colliding bubbles separate apart from each other after collision and that only a fraction of collisions lead to coalescence. Hence, it is reasonable to introduce coalescence efficiency additionally for the description of the coalescence process. Liao and lucas (2010) reported that at least three models have been used for the calculation of coalescence efficiency namely, energy model, critical approach velocity model and the film drainage model.

2.4.2 Energy models

The energy model was originally proposed by Howarth (1964, 1967) and it was confirmed by the optical records of coalescence in dispersion (Park et al. 1975; kuboi et al., 1972), which found that significant fraction of collisions result in immediate coalescence and the probability increases with increasing energy of collision. Sovova (1981) developed a model which related the kinetic collision energy E_{kin} to the interfacial energy E_{σ} of the bubble so that:

$$\lambda_1(d_1, d_2) = \exp\left(-C_{21} E_{\sigma} / E_{kin}\right) \tag{2.63}$$

The interfacial energy of drops is proportional to the interfacial tension and drop surface area such that:

$$E_{\sigma} = \sigma\left(V_1^{2/3} + V_2^{2/3}\right) \tag{2.64}$$

Whereas the kinetic collision energy E_{kin} is assumed to be proportional to the average volume $\bar{V}$ and relative velocity of two colliding drops u_{rel} such that:

$$E_{kin} = \frac{1}{2}\rho_d \bar{V} u_{rel}^2,\ \bar{V} = V_1 V_2 / (V_1 + V_2) \tag{2.65}$$

Finally the expression for the coalescence efficiency becomes:

$$\lambda_1(d_1, d_2) = \exp\left(- C_{22} \frac{\sigma\left(V_1^{2/3} V_2^{2/3}\right)(V_1 + V_2)}{\rho_d \varepsilon^{2/3} V_1 V_2 \left(V_1^{2/9} + V_2^{2/9}\right)} \right) \tag{2.66}$$

2.4.2.1 Critical approach velocity model

From the energy model, it is deduced that coalescence will happen immediately once the approach velocity of the two collision bubbles exceeds a critical value at the instant of collision. However, Doubliez (1991) and Duineveld (1994) from their demonstration observed that coalescence behaviour favours gentle collision. A simple expression was used by Lehr et al. (2002), Lehr and Mewes (1999) for the observed relationship between coalescence efficiency and approach velocity

$$\lambda(d_1, d_2) = \max\left(\frac{u_{crit}}{u_{ret}}, 1 \right) \tag{2.67}$$

The critical velocity u_{crit} can be determined experimentally. From equation 2.31 one can see that the efficiency is larger than or equal to unity, i.e. $\lambda(d_1, d_2) \geq 1$. Again, it can be said that when the relative velocity approaches to the limit of zero, the coalescence efficiency will be a value of infinity, which is very big. Therefore, the correct correlation will be

$$\lambda(d_1, d_2) = \min\left(\frac{u_{crit}}{u_{rel}}, 1 \right) \tag{2.68}$$

2.4.2.2 Film drainage model

The film drainage model determines the coalescence efficiency from two characteristic time scales, i.e. the contact time and the drainage time, which is the time required for the intervening film between the bubbles to thin down to critical thickness. By assuming that the coalescence and contact time are random variables, Ross (1971) applied the probability density function of a normal distribution for the computation of coalescence efficiency as:

$$\lambda(d_1, d_2) = \frac{1}{2}\exp\left(-\frac{t_{drainage}}{t_{contact}}\right)\exp\left(\frac{1}{2}\frac{\delta_{drainage}^2}{t_{contact}^2}\right) \times erfc\left(\frac{\sqrt{2}}{2}\frac{\delta_{drainage}^2 - t_{drainage}t_{contact}}{t_{contact}\delta_{t_{drainage}}}\right) \quad (2.69)$$

Coulaloglou (1975) simplified Ross model (equation 2.69) by assuming that the coalescence time is not distributed although the contact time remains a random variable, that is, $\sigma_{tdrainage} = 0$ and obtained an expression of the coalescence efficiency as:

$$\lambda(d_1, d_2) = \exp\left(-\frac{t_{drainage}}{t_{contact}}\right) \quad (2.70)$$

Although a few criticisms appear in literature on the validity of the two timescales, the assumption of random variables as well as normal distribution (Das and Kumar, 1987), the film drainage model is up to now the most popular one and a number of researches have been focused on the calculation of the contact time and drainage time.

Among them, the Prince and Blanch (1990) model simplified the film drainage model and obtained the drainage time expression as:

$$t_{drainage} = \left(\frac{(d_{ij}/2)^3 \rho_i}{16\sigma} \right)^{1/2} In\left(\frac{h_o}{h_f} \right) \tag{2.71}$$

The contact time $t_{contact}$ was calculated as (Levich, 1962):

$$t_{contact} = \left(\frac{d_{ij}/2}{\varepsilon^{1/3}} \right)^{2/3} \tag{2.72}$$

The equivalent diameter d_{ij} is calculated as suggested by Chesters and Hoffman (1982) to be:

$$d_{ij} = \left(\frac{2}{d_i} + \frac{2}{d} \right)^{-1} \tag{2.73}$$

The parameter h_o and h_f respectively represent the initial film thickness when collision begins and critical film thickness at which rapture occurs which have been set to $h_o = 1 \times 10^{-4} m$ and $h_f = 1 \times 10^{-8} m$

2.4.3 Mechanism of fluid particle breakup

Figure 2.3 Classification of break-up frequency models based on break-up mechanism. (Liao and Lucas 2009).

The breakup of fluid particles in turbulent dispersions is influenced by the continuous phase hydrodynamics and interfacial interactions. In general, breakup mechanism can be expressed as a balance between external stresses from the continuous phase, which attempt to destroy the fluid particle, and the surface stress of the particle plus the viscous stress of the fluid inside it, which restores its form. This balance leads to the prediction of a maximum stable particle diameter (Kocamustafaogullari et al., 1995; Revankar et al., 2001. According to Liao et al., (2009), breakup mechanisms can be classified into four main categories: (1) turbulent fluctuation and collision; (2) viscous shear stress; (3) shearing-off process; (4) interfacial instability. In the case of turbulent flow, the breakup of fluid particles is caused mainly by turbulent pressure fluctuations along the surface, or by particle-eddy collisions. The particle can be assumed to modify its spherical form with the fluctuation of the surrounding fluid or due to collisions with eddies. Deformation of the particle starts when the amplitude of the oscillation is close to that required to make the particle surface unstable, causing a stretch in one direction that leads to the particle neck contracting further and fragments finally into two or more daughter particles. The breakup mechanism can be expressed as a balance between dynamic pressure τ_t (i.e. turbulence-induced destroying stress or energy) and its surface stress τ_s (i.e. the restoring stress or energy related to the surface tension). Whether or not the particle will break depends on the extent of the deformation or the weber number We where:

$$We = \frac{\tau_t}{\tau_s} = \frac{\rho_l u_{rel}^2 D_b}{\sigma} \tag{2.74}$$

In literature, one can distinguish between five cases of breakup criterion in turbulent flow, namely:

(a) Turbulent kinetic energy of the particle greater than a critical value (Coulaloglou and Tavlaride, 1977; Chatzi et al., 1987, 1989, 1983);

(b) Velocity fluctuation around the particle surface greater than a critical value (Alopaeus et al., 2002a, b; Narimhan and Gupta, 1979);

(c) Turbulent kinetic energy of the hitting eddy greater than a critical value (Lee et al., 1987a, b; Luo and Svendsen, 1994; Martinez-Bazan et al., (1999a, b);

(d) Inertial force of the hitting eddy F_e greater than the interfacial force of the smallest daughter particle F_σ (Lehr and Mewes, 1999; Lehr et al., 2002);

(e) Combination of the criterion (c) and (d), such in Wang et al., (2003) and Zhao and Ge (2007).

According to Liao et al., (2009), the critical energy is defined, arbitrarily by the above authors, as surface energy of the parent particle (Lee et al., 1987a, b; Prince and Blanch, 1990; Martinez-Bazan et al., 1999a, b) or the increase in the surface energy before and after breakup (Luo and Svendsen, 1996; Wang et al., 2003; Zhao and Ge, 2007), or the mean value of the surface energy increase for breakage into two equal-size daughters and into a smallest and a biggest one (Tsouris and Tavlarides, 1994).

In the last decades, analyses and modelling of breakup process has received considerable attention and a large number of models for the breakup frequency and daughter size distribution have been published as classified in Figure 2.3. It is important however, to point out that in most cases; the continuous flow field is a turbulent flow. Thus, the study

of breakup frequency is focused on the turbulent flow. Furthermore, the turbulent fluctuation is assumed arbitrarily to be the dominant breakup mechanism and the effects of viscous force, relative velocity and interfacial instability on breakup phenomena are usually neglected without any further validation.

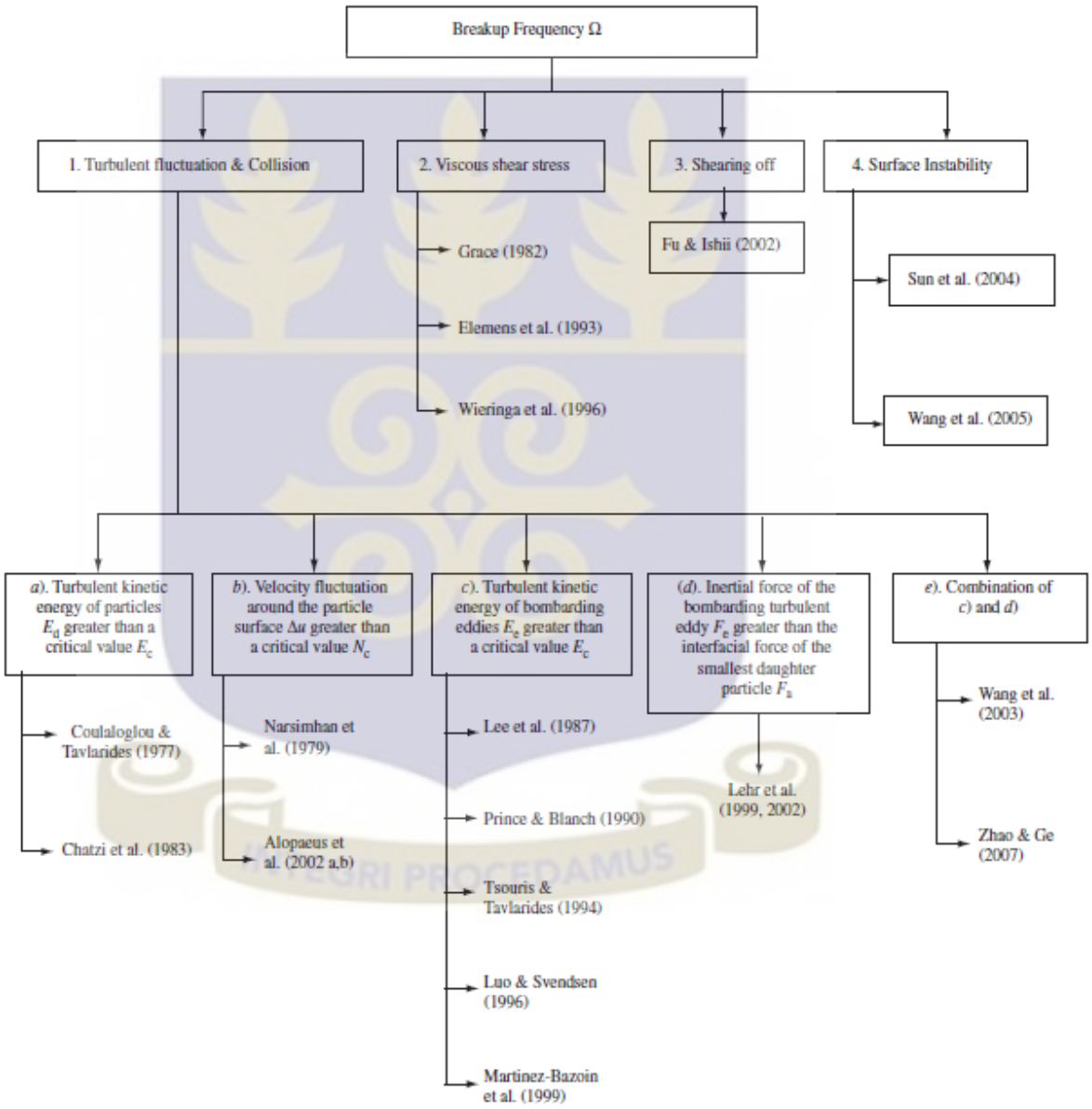

Figure 2.5: Classification of break-up frequency models based on break-up mechanism. (Liao and Lucas 2009).

2.4.3.1 Models for fluid particle Breakup frequency $\Omega_{tur}(\xi;\xi)$

A pioneering phenomenological model was proposed by Coulaloglou and Tavlarides (1977), which was based on the turbulent nature of the liquid-liquid dispersion. Again, their observation shows that, the drop oscillates and deforms due to local pressure fluctuations. The fundamental fact here is that, the to and fro deform drop will break if its kinetic energy E_d, transmitted from drop-eddy collisions, is greater than its surface energy E_c. The breakup frequency is defined as:

$$\Omega(\xi_i) = \left(\frac{1}{breakup\ time}\right).\left(\frac{fraction\ of}{drops\ breaking}\right) \tag{2.75}$$

where $\Omega(\xi_i)$ is the total number of particles of size ξ_i.

One can determined the breakup time from the isotropic turbulence theory by assuming that the motion of daughter drops is the same as that of turbulent eddies. Again, the fraction of drops breaking is assumed proportional to fraction of drops that have a turbulent kinetic energy greater than their surface tension, therefore the equation can be expressed as:

$$\Omega(\xi_1) = c_1 v_1^{-2/3} \varepsilon^{1/3} \exp\left[-\frac{c_2 \sigma}{\rho_g \varepsilon^{2/3} v_i^{5/3}}\right] \tag{2.76}$$

Coulaloglou and Tavlarides modified an expression to account for the "damping" effect of droplets on the local turbulent intensities at high holdup fractions and this expression is:

$$\Omega(\xi_i) = c_3 v_i^{-2/3} \frac{\varepsilon^{1/3}}{1+\alpha} \exp\left[-\frac{c_4 \sigma (1+\alpha)^2}{\rho_g \varepsilon^{2/3} v_i^{5/3}} \right] \tag{2.77}$$

where v_1 is the distance separating the two points, c_1, c_2, c_3, and c_4 are constant to be determined experimentally.

Although many previous model considered the collision between eddies and drops was the dominant reason for breakup, Prince and blanch decided to determine the breakup frequency by making an analogy to collisions ideal gases and examining the interaction of bubbles with turbulent eddies. Prince and Blanch (1990) decided to compute the breakup frequency by multiplying the collision frequency $\vartheta(d_1, d_2)$ with collision efficiency $P_b(d_i, d_e)$, i.e.

$$\Omega(\xi_i) = \int \vartheta(d_i, d_e) P_b(d_i, d_e) d(d_e) \tag{2.78}$$

where d_e is the eddy length scale.

The collision frequency can be defined as the volume swept in unity time, which is equal to the product of the cross-sectional area S, the relative velocity between bubbles and eddies u_{rel} and the number density of eddies with size d_e, n_e, i.e:

$$P_b(d_i, k) = u_{rel} . S . n_e \tag{2.79}$$

Again, the efficiency $P_b(d_i k)$ is assumed equal to the probability that turbulent eddies have efficient energy to rapture a bubble. The critical Weber number We_{cr} which is considered as constant for given system can be used to determine the critical or minimum energy E_{cr} while the random distribution of kinetic energy E_e in eddies obeys a normal function. Taking the eddy energy as proportional to the square of its velocity yields a function of the following form for the breakup efficiency $P_b(d_i, k)$:

$$P_b(d_i, k) = \exp\left(-\frac{r_{cr}^2}{r_e^2}\right) \tag{2.80}$$

Finally, when the critical Weber number We_{cr} is given 2.3 for air bubbles in water, the integral in equation (2.80) can be rewritten as:

$$\Omega(\xi_i) = \int_{k_{\min}}^{k_{\max}} \frac{0.14\pi}{16}\left(d_i + \frac{2}{k}\right)^2\left(d_i^{2/3} + \left(\frac{2}{k}\right)^{2/3}\right)^{1/2} \varepsilon^{1/3} \times \exp\left[-\frac{1.18}{(2)^{2/3}\rho_c d_i \varepsilon^{2/3}}\right] k^2 dk \tag{2.81}$$

where k is the wave number of eddies, related to the eddy size by $k = 2/d_e$.

In Prince and Blanch (1990) it was noted that the upper limit of equation (2.81) becomes infinitely large as the eddy size approaches zero. Again, with the premise of the inertial subrange, they set the minimum eddy size arbitrarily to 20% of the bubble diameter. However, Lasheras et al., (2002) reported that the result depends on sensitively on this upper limit.

Luo and Svendsen (1996) criticize all previous model by pointing out the experimental costs needed for determining unknown parameters. However, Prince and Blanch (1990) proposed a new theoretical model for breakup frequency based on the kinetic gas theory.

$$\Omega(\xi,\xi)=\int_0^{\infty}\vartheta(d_i,d_e)P_b(d_i,d_j,d_e)d(d_e) \tag{2.82}$$

Equation (2.82) was used to calculate the collision frequency between a particle of size d_i and eddies of a size between d_e and $d_e+d(d_e)$, but the expression for the velocity and number density of eddies is slightly different. One can say that, the computation of Break-up efficiency $P_b(d_i,d_j,d_e)$ is also similar to the $P_b(d_i,d_e)$ of Prince and Blanch (1990) and Tsouris and Tavlarides (1994). Therefore, the unique difference is the critical energy E_c, which is defined as the increase in surface energy during the breakage $\Delta\bar{E}(d_i)$. However, the breakup frequency of a particle with size d_i that breaks into daughters with sizes ξ_j and $\xi_j-\xi_j$, $\Omega(\xi_i,\xi_j)$, is given as:

$$\Omega(\xi_i\xi_j)=0.923(1-\alpha)\left(\frac{\varepsilon}{d_i^2}\right)^{1/3}\int_{\Lambda_{\min}}^{1}\frac{(1+\Lambda)^2}{\Lambda^{11/3}}\exp\left(-\frac{\Delta\bar{E}_i(d_i)}{\bar{E}(d_e)}d\Lambda\right) \tag{2.83}$$

where $\Lambda=\frac{d_e}{d_i}$, $\Lambda_{\min}=\frac{d_{\min,e}}{d_i}$, $\frac{d_{\min,e}}{\eta}\approx 11.4-31.4,\eta$ is the Kolmogorov microscale.

Finally, the total breakup frequency of particles with size d_i is given as:

$$\Omega(\xi)=\frac{1}{2}\int\Omega(d,d_1)df_v \tag{2.84}$$

Where $f_v = \frac{d_i^3}{d_j^3}$ and $0 \le C_f = f_v^{2/3} + (1+f_v)^{2/3} - 1 \le 0.26$ and this depends on the daughter drop diameter.

Luo and Svendsen. (1996) proposed a turbulent induced break-up model to describe break-up frequency, $\Omega_{tur}(\xi)$ based on kinetic gas theory

$$\Omega_{tur}(\xi_i, \xi_j)\, 0.923 C_2 (1-\alpha_g) \left(\frac{\varepsilon}{d_i^{\,2}}\right)^{1/3} \int_{\varsigma_{\min}}^{1} \frac{(1+d)^2}{d^{11/3}} e^{-x} d\Lambda \tag{2.85}$$

$$x = \frac{6\sigma\left[\left(\frac{m_\xi}{m_{\xi'}}\right)^{2/3} + \left(1-\frac{m_\xi}{m_{\xi'}}\right)^{2/3} - 1\right]}{\rho_l \varepsilon_l^{2/3} \xi'^{5/3} \varsigma 11/3} \tag{2.86}$$

where $\varsigma_{\min}$ is the dimensionless size of is eddies in the inertial sub-range of isotopic turbulence. The lower limit of the integration is given by:

$$\varsigma_{\min} = (11.4 \sim 31.4)\,(\mu_l / \rho_l)^{1/4} / (\varepsilon^{1/4} \xi') \tag{2.87}$$

In summary, the breakup frequency model is based on bubble eddy collision mechanism which depends on the same arguments made on kinetic theory of gases.

Finally, using poly-dispersed approach, numerical investigation was done for the interfacial force models, bubble induced turbulence models, the setup for the MUSIG model for modelling poly-depersed flow and modelling of calibration factor will be discussed in the next chapter.

Chapter 3

Methodology

For accurate modelling of flow regimes, one could not under estimate the effect of modification factors of coalescence and breakup models, therefore, in this chapter three different model expressions of modification factors for coalescence model from literature have been model into the ANSYS CFX command language and their estimate is validation against experimental data of vertical isothermal bubbly flow conducted by Monros et al., (2013). In view of this, the software used, mesh sensitivity analysis, and the boundary condition are discussed in this Chapter. This is coupled with different model expressions of calibration factors for coalescence models discussed in literature.

3.1 Upward Turbulent Adiabatic Bubbly Flow Experimental Data from Monros et al., (2013)

The results of the simulations presented in the next Chapter have been compared against the experimental data as reported by Monros et al., (2013). The experimental facility was built to study the effects of temperature variation in the bubbly to slug transition flow. These facilities are distinguished by geometry of the test channel (which may be circular or rectangular, with various diameter sizes and length), orientation and flow direction (vertical or horizontal, counter-current). They are also distinguished by working fluids (water, air, oil-nitrogen mixtures of alcohol, hot-air, viscous oils, etc.), and by the conditions under which the tests are performed (adiabatic, atmospheric pressure, pressurized, etc). Another important difference in the experimental facilities is the

techniques used in measuring the characteristics of two-phase flow, for example using visualization techniques or using invasive techniques.

The set-up of the experimental facility built and operated at the Department of Mechanical Engineering and Construction, University Jaume I, Castellon, Spain is schematically illustrated in figure 3.1.

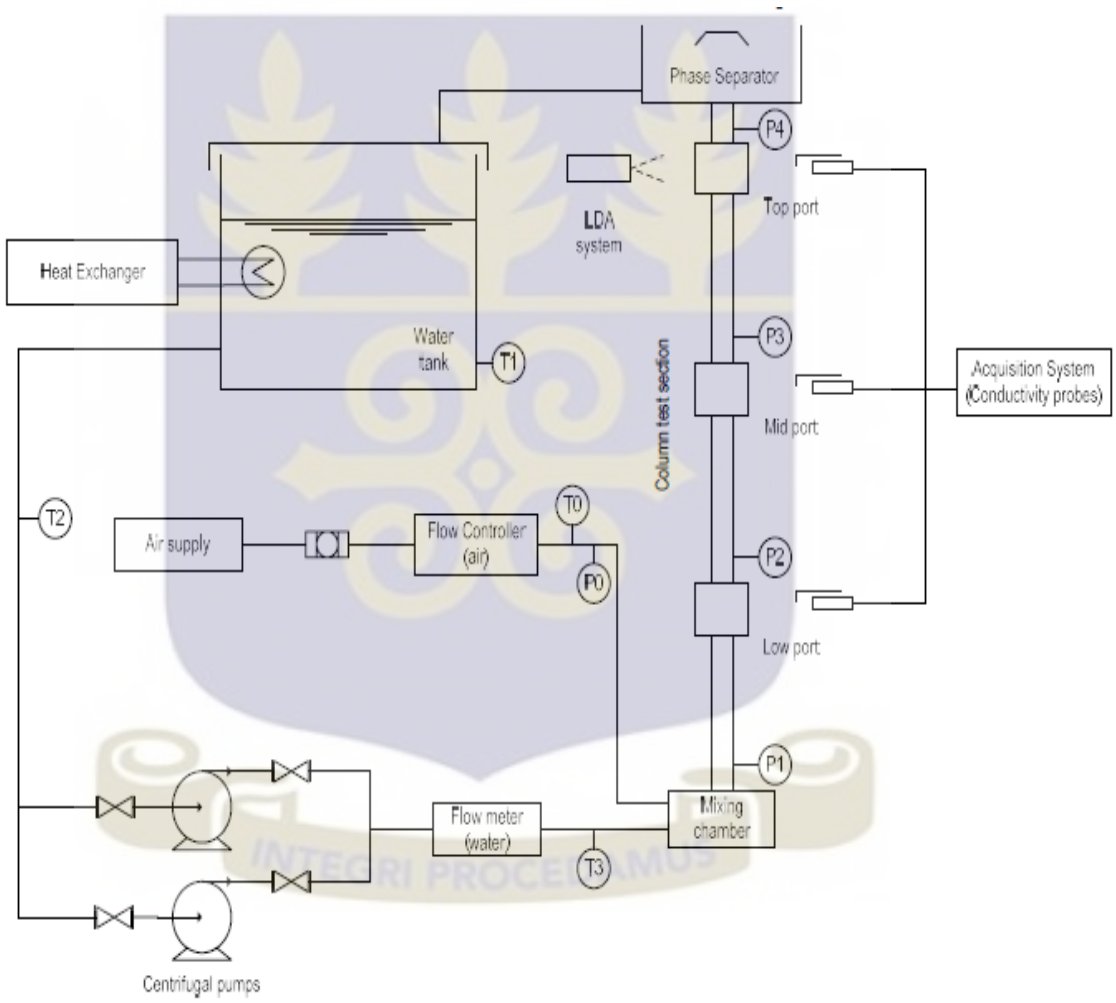

Figure 3.1: General overview of the experimental facility (Monros et al. 2013)

Experiments were carried out in an upward air-water flow configuration. The test section was a round transparent tube made of Plexiglas, 52mm inner diameter and 5500 mm

length. The local flow measurements using a four-sensor conductivity probe were carried out at axial locations of 1166 mm (Low Port, L/D=22.4), 3176 mm (mid Port, L/D=61) and 5131 mm (Top Port, L/D=98.7). The water was circulated in the loop by a pair of centrifugal pumps, controlled with a frequency controller device. The bubbles, with diameters ranging from 1 to 4 mm (depending on the flow condition), were generated by a sparger, with an average porosity of 40 microns, located in the base of mixing chamber. Pressure transducers and temperature sensors were installed in order to register the pressure and temperature of both phases. The superficial velocity of the liquid phase was measured using a magnetic flow meter (Badger model M100), which provides the superficial velocity of the liquid phase at the inlet of the test column section. Injected air superficial velocity was measured and controlled with a Bronckhorst EL-FLOW flow controller. In order to control water temperature a heat exchanger (Euroklimat R407C SMART 400/30/50) was connected to the water tank so that the system temperature is maintained at a constant temperature in the range between 15 to 30 ^{0}C. Pressure sensors were installed in each of the measurement port and also before the mixing chamber. These sensors have ranges of 0-1 bar to the bottom port, and 0-250mBar for the other two ports. The interfacial area concentration, void fraction and bubble chord length were measured using four-sensor conductivity probe. The laser Doppler Anemometry (LDA) equipment consisting of a 0.5W Ar+ Ominichrome Laser, Dantec Fiber flow beam separator, Dantec FVA 58N40 processor and PC using the software "Floware" for data acquisition was used to measure the liquid velocity and turbulent kinetic energy. The schematics of the four-sensor conductivity probe and LDA measurement system is shown in Figure 3.2.

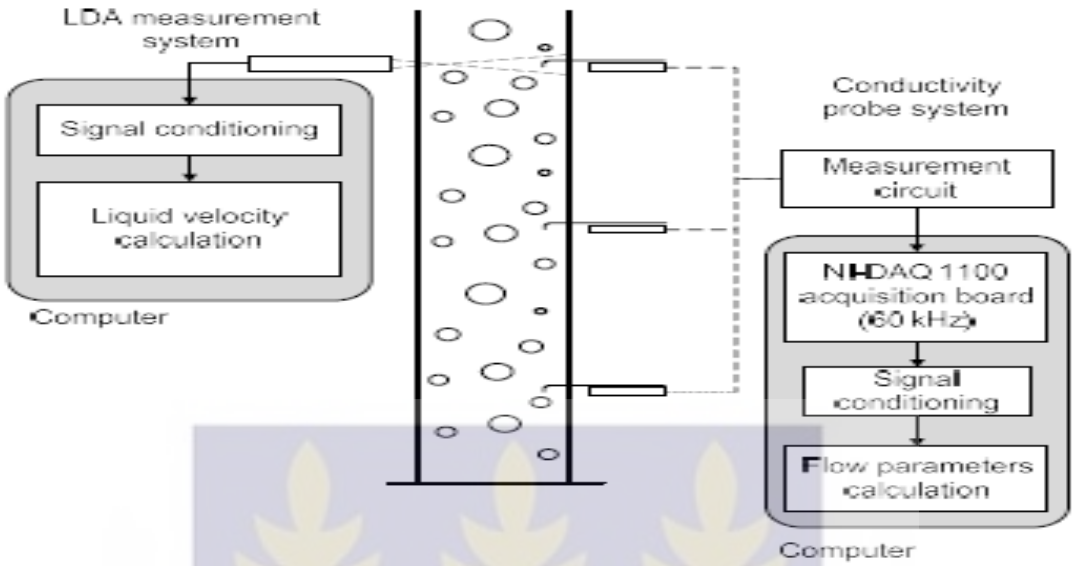

Figure 3.2: Conductivity probe and LDA measurements system (Monros et al. 2012)

The four-sensor conductivity probe is basically a phase identifier and is used to acquire the time-averaged local two-phase flow parameters of the bubbles. It consists of four sensors made of insulated copper, with a diameter of 0.25 mm. The vertical distance between main and auxiliary tips was about 1.5 mm.

3.2 Matrix for Model Testing

The experimental points considered for the validation of the numerical results presented in Chapter 4 and their superficial velocities are represented in the flow regime map proposed by Taitel et al., (1980) and Serizawa & Kataoka (1986) as shown in Figure 3.3. The data have been collected at a pressure about 1atm and a temperature of 22^0C (Yamoah, 2014). The experiments were performed by changing the superficial velocity of one phase and keeping the superficial velocity of the other phase constant as indicated in Figure 3.3.

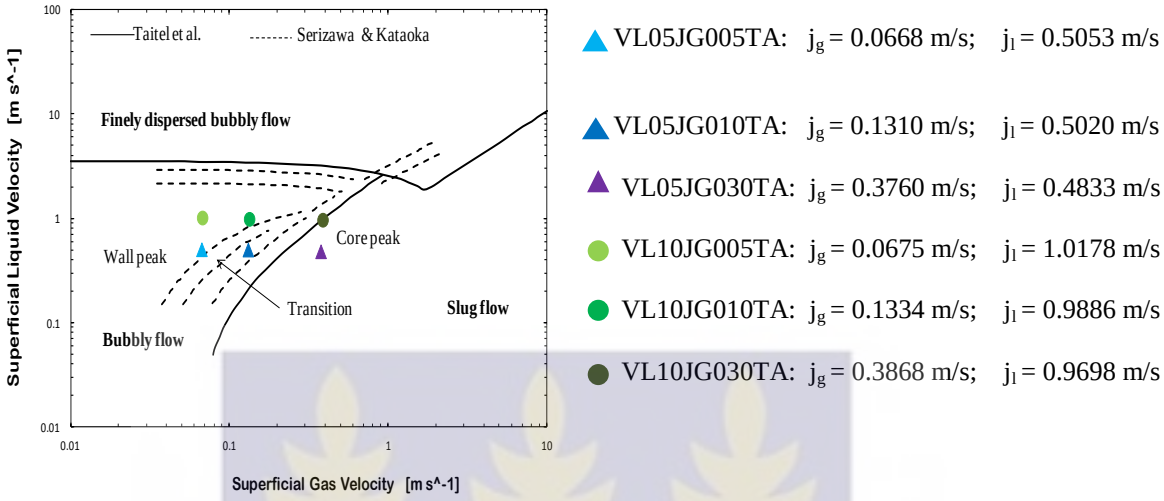

Figure 3.3: Flow regime map for vertical pipes. (Yamoah, 2014).

3.3 The Computational Fluid Dynamics Code ANSYS CFX

ANSYS CFX is a general purpose Computational Fluid Dynamics (CFD) software suite that combines an advanced solver with powerful pre-and post-processing capabilities and includes the following features:

- An advanced coupled solver that is both reliable and robust.
- Full integrating of problem definition, analysis, and results presentation
- An intuitive setup process, using menus and advanced graphics.

Computational fluid dynamics is the analysis of engineering systems involving fluid flow, heat transfer and associated phenomena, by means of computer-based simulations, solving equations for mass, momentum, energy, turbulence and concentration with specified conditions on the boundary of that region. In CFD codes, a number of different solution methods are used with the most common, and the one on which CFX is based, known as the finite volume method. In this method, the region of interest is divided into

small sub-regions, called control volumes. The equations are discretized and solved iteratively for each control volume. As a result, an approximation of the value of each variable at specific points throughout the domain can be obtained (CFX 14.5 2012).As shown in Figure 3.4, ANSYS CFX is a suite composed of several packages. They are essentially three. The "pre-processor" to define computational regions, the initial and boundary conditions, materials properties, the physical models and the numerical schemes. The "solver" used to solve the variables of the problem and to manage partitioning and memory allocation. The "post-processor" to create 2D or 3D plots of the main significant variables of the problem and to export the data for further analysis..

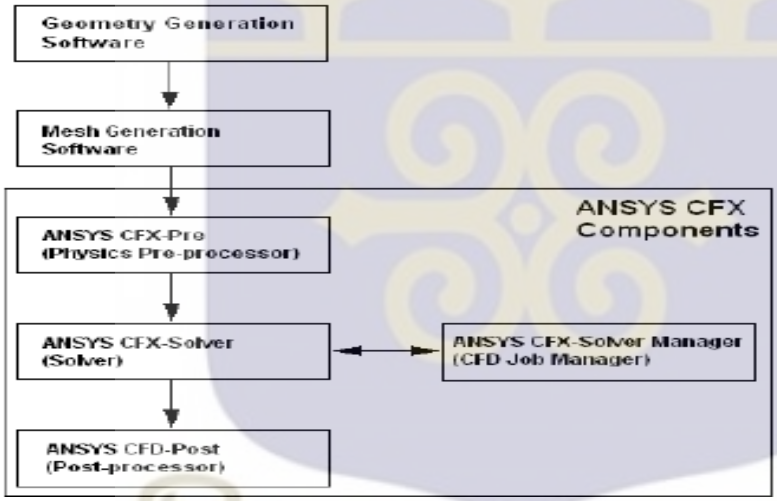

Figure 3.4: Overview of ANSYS CFX code structure (CFX-14.5, 2012).

3.4 Two-phase Flow Simulation Methods in ANSYS CFX

ANSYS CFX is able to solve two-phase flow problems by using either Eulerian-Eulerian multiphase model or Langrangian Particle Tracking multiphase model. In this thesis, the Eulerian-Eulerian multiphase model has been used.

Within the Eulerian-Eulerian formulation, certain inter-phase transfer terms used in the momentum, heat, and other inter-phase transfer models can be modelled using the CFX-14.5, 2012):

- Particle Model
- Mixture Model
- Free surface Model

(Also the calculation of the interfacial area density used for all inhomogeneous transfer models for a given fluid pair is calculated according to one of these models (CFX 14.5, 2012). Inhomogeneous multiphase flow in this case refers to where separate velocity fields and other relevant fields exist for each phase. However, the pressure field is shared by both phases and they interact through the inter-phase transfer terms. The simulation performed in this study is based on the two-fluid approach which has already been introduced in Chapter two (Section 2.2).To account for the inter-phase transfer terms in the momentum equation, the particle model has been used. The particle model considers one of the two phases as continuous and the other dispersed. The dispersed phase can be considered as:

- Mono-dispersed
- Poly-dispersed (MUltiple SIze Group, MUSIG)

If the gas is considered as the dispersed phase, then in the mono-dispersed approach, all the bubbles are assumed to have the same spherical form and the same average diameter which can be a constant or an expression dependent on local parameters. Furthermore, the bubbles share the same dispersed phase velocity field. Thus, for a two-fluid system, the equations to be solved are in total 11 divided as follows:

- Momentum of the liquid phase: 3
- Momentum of the gas phase: 3
- Pressure: 1
- Mass of Liquid: 1
- Mass of gas: 1
- Turbulence in the liquid phase: 2

On the other hand, in the case of poly-dispersed approach, if the gas is considered to be the dispersed phase, then all the bubbles present in the system are supposed to share the same spherical form but not the same average bubble diameter. In this case, the bubbles are divided into classes and the initial bubble size distribution which has a strong influence on the inter-phase transfer is defined as a boundary condition. The bubble groups can share the same velocity field (Homogeneous MUSIG) or they can be associated to different velocity field (Inhomogeneous MUSIG). The intergroup bubble transfer mechanism is simulated as presented in Chapter 2 (Section 2.4) by means of coalescence and breakup source and sink terms. They determine the changes in the bubble group size fractions as a result of breakup and coalescence process. In the case of a two-fluid system (homogeneous MUSIG) considering n bubble size groups the equations to be solved are in total **11+n** divided as follows:

- Momentum of the liquid phase: 3
- Momentum of the gas phase: 3
- Pressure: 1
- Mass of Liquid: 1
- Mass of gas: 1

- Turbulence in the liquid phase: 2
- Bubble group size fraction: n

3.5 Mesh Generation

The mesh used in this study has been created with the unstructured hexahedral meshing module using ICEM CFD 14.5 meshing software. In order to reduce computational cost, radial symmetry has been assumed; consequently a 5-degree wedge section of the pipe was adopted as the solution domain with symmetry boundary conditions at both vertical sides, instead of whole pipe domain. Sari et al. (2009), Liao et al. (2011) and Yamoah. (2014) already used the 5-degree calculation mesh to simulate experiments related to upward vertical bubbly flow conditions. The computational mesh and geometry is shown in Figure 3.5.

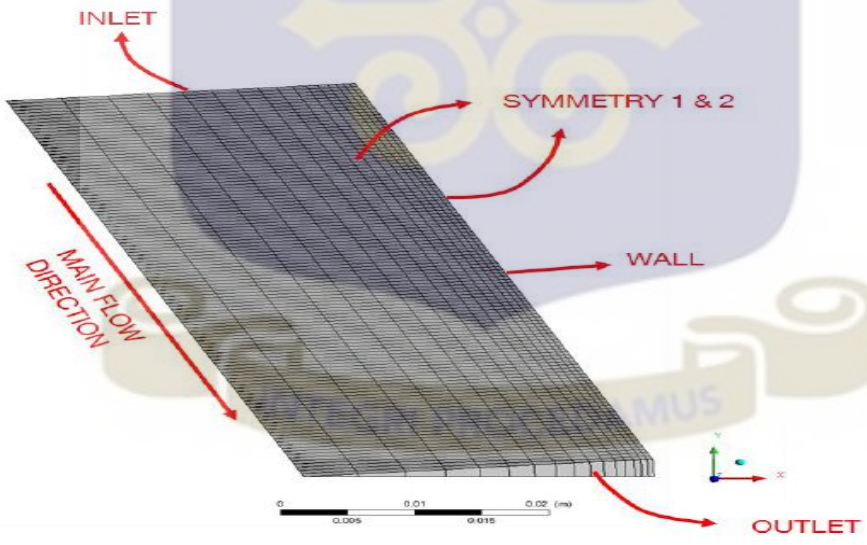

Figure 3.5: Mesh distribution of computational model

In developing the mesh, the general recommendations of the best particle guidelines for the use of CFD in nuclear reactor safety applications (Best Guidelines, 2007) for

generating high quality grids were followed to ensure that a good quality mesh was used for the simulation.

3.5.1 Mesh Sensitivity Analysis

The assessment of the mesh quality before performing a CFD analysis is very important. Thus, in order to find an ideal mesh for the computational analysis, the effect of changing grid size was investigated by Yamoah (2014) which was adopted in this study. Several meshed were prepared to study the effects of the spatial discretisation on the numerical results. The mesh sensitivity analysis has been performed using the case define as VL10JG005TA. In Table 3.1 and 3.2 the details of the mesh resolution is presented.

Table 3.1: Mesh details- Radial elements variation

Type	Radial elements [-]	Axial elements [-]	Nodes [-]	Calculation Time [s]
Mesh A	17	286	9438	2874
Mesh B	27	286	15158	4116
Mesh C	37	286	20878	4063
Mesh D	45	286	25454	3760
Mesh E	53	286	30030	4006

Table 3.2: Axial elements variation

Type	Radial elements [-]	Axial elements [-]	Nodes [-]	Calculation Time [s]
Mesh B	27	286	15158	4116
Mesh F	27	821	43513	3320
Mesh G	27	411	21783	3944
Mesh H	25	206	10918	3501

The effect of the different mesh on the calculation results have been shown in Figure 3.6 and 3.7. The plotted data have been extracted at a height of 3.965 m and they represent the behaviour at any other axial point.

From Figure 3.6 and 3.7, it can be observed that the best combination between acceptability of the results and computational time is represented by Mesh G in Table 3.2. In view of the observed effect of grid size, the numerical investigation performed in this study have been carried out by using a hexahedral mesh with 27 radial elements and 411 axial elements giving a total of 21783 nodes that represents a 5^0 wedge section of the pipe

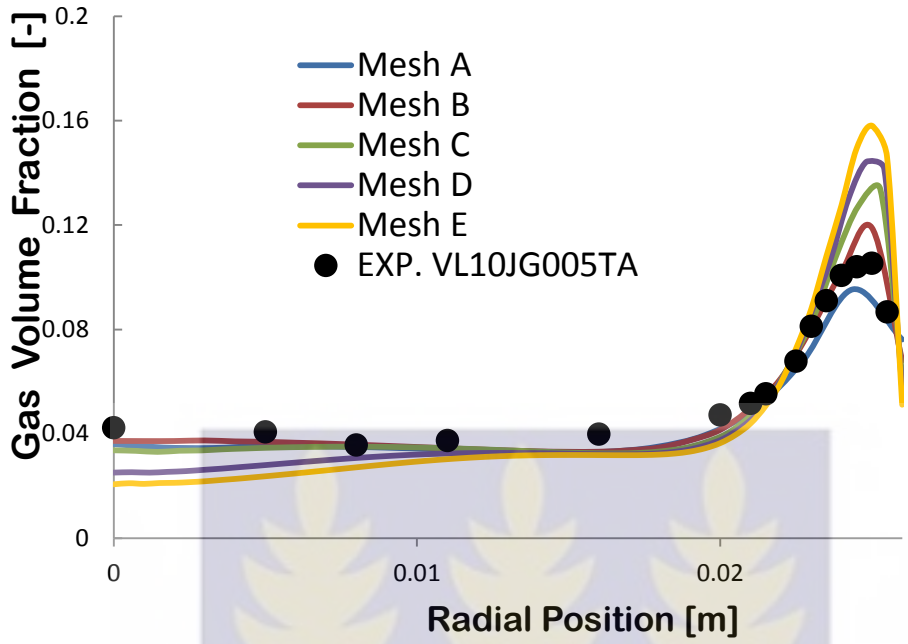

Figure 3.6 Influence of radial node distribution on the gas volume fraction radial profile (Yamoah, 2014)

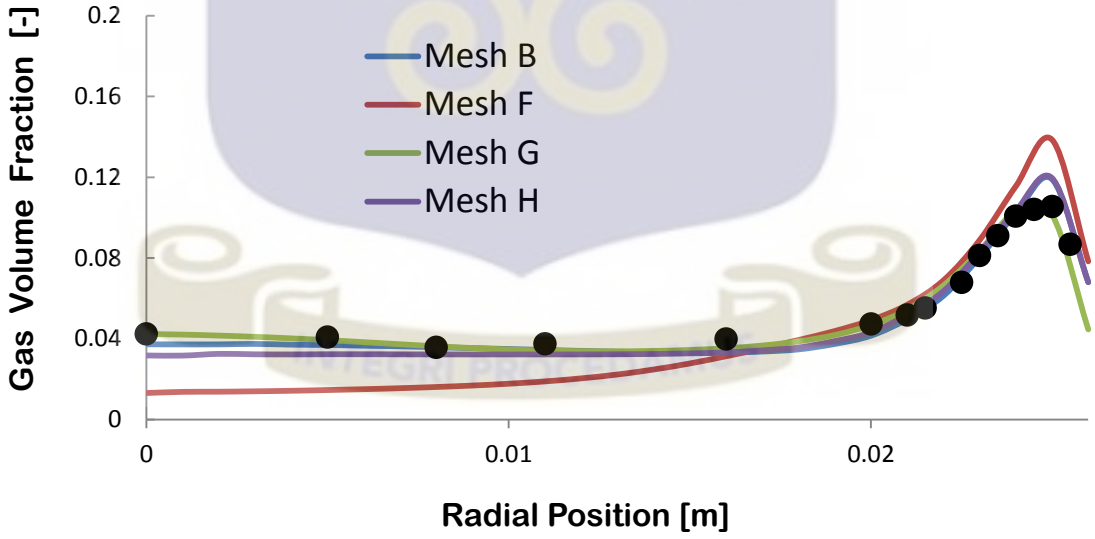

Figure 3.7 Influence of the axial node distribution on the gas volume fraction radial profile (Yamoah, 2014)

3.6 Definition of Boundary Conditions, Turbulence and Discretisation Scheme

The computational model in this study consists of five fluid boundaries namely; inlet, outlet, wall, symmetry 1 and symmetry 2. The boundary conditions at the boundaries have been set as follows.

1) Outlet: At the outlet the relative pressure is set to zero. What this means is that, the system pressure equals the atmospheric pressure.

2) Inlet: The experimental radial profiles measured at the entrance of the experiment have been set as inlet conditions for the following variables:

- Gas Volume Fraction
- Liquid Volume Fraction (1- Gas Volume Fraction)
- Gas Velocity
- Liquid Velocity

In addition, the size fractions of N bubble groups have been set as a boundary condition at the inlet.

3) Wall: For the liquid phase, a non-slip boundary condition was set and for the gas phase, a free-slip boundary condition was set up.

Symmetries: For symmetry planes, no particular model was set for them.

A Reynolds Averaged Navier Stokes (RANS) turbulence model, based on the SST model introduced in Chapter 2 (Section 2.1.1) for the liquid phase has been used as explained. A zero equation turbulence model for the gas phase was considered because it was simple to

implement and use and can produce approximate results very quickly. The bubble induced turbulence has been taken into account based on the model of Sato et al., (1981) analysis. In each cell of the computational domain the governing equation were solved under steady condition and the code stores the discrete values at the centre of the cell. These values are interpolated from the centre of the cell to face values at specific points through discretisation schemes as listed in Table 3.3.

Table 3.3: Discretisation scheme used in this study

Quality	Scheme
Advection Scheme	High resolution
Turbulence Numerics	First Order
Continuity	High Resolution
Momentum	High Resolution
Turbulence Eddy Frequency	Upwind
Turbulence Kinetic Energy	Upwind
Volume Fraction	High Resolution

Stephen Yamoah et al., (2015) performed analysis of convergence effect on root mean square (RMS) value of 10^{-4} and 10^{-5}. They concluded that the reduction of RMS limit to stop convergence introduces slight changes in the void and IAC profiles, but this takes place at the expense of a huge increase in calculation time (typically by a factor of 10). Thus, for all flow conditions simulated in this study, reliable convergence criterion based

on the root means square (RMS) residual of 1×10^{-4} was adopted for the termination of numerical calculations.

3.7: Modelling of Isothermal Gas-liquid Bubbly Flow Using the Homogeneous MUSIG Model.

The MUltiple Size Group method is based on population balance method as presented in Section (2.3) and the two fluid modelling approach. The dispersed phase is divided into M size fractions. The population balance equation is applied to describe the mass conservation of the size fraction taking into account the inter-fraction mass transfer resulting from bubble coalescence and break-up. This model approach allows a sufficient number of size fraction groups required for the coalescence and break-up calculation to be used and has found a number of successful applications to large-scale industrial multiphase problem. Nevertheless, the assumption also restricts its applicability to homogeneous dispersed flows, where the slip velocities of particles are almost independent of particle relaxation time is sufficiently small with respect to inertia time scale. Thus, the asymptotic slip velocity can be considered to attain almost instantaneously. Key to the success of this method is the number of size groups used for the simulation and the size group fractions. In order to find an ideal number of size groups needed to describe a meaningful distribution and for a more accurate measure of the interfacial area density, Yamoah (2014) investigated sensitivity of the number of size groups by dividing the bubble diameters equally into 5, 10, 15, and 20 size groups. The investigations showed that no appreciable difference was found for the predicted gas volume fraction, interfacial area concentration Sauter mean bubble diameter, gas velocity and the liquid velocity and that the subdivision into 10 size groups was

sufficient. Thus, the subdivision into 10 size groups has been adopted in this study and hence all simulations performed in this thesis are based on the discretisation of the bubble sizes into 10 groups as shown in Table 3.4

Table 3.4: Diameter of each bubble class tracked in the simulation

Size Group	Size Group Diameter (mm)
Group 1	1.25
Group 2	2.20
Group 3	3.15
Group 4	4.10
Group 5	5.05
Group 6	6.00
Group 7	6.95
Group 8	7.90
Group 9	8.85
Group 10	9.80

Size fraction is defined as the ratio of volume of a specific size group of bubble to the total void fraction of the gas phase. Similar to void fraction, this parameter also range from 0 to 1. If the gas phase is divided into i groups depending on size, then the size fraction of i^{th} group is f_i was computed as

$$f_i = \frac{\alpha_i}{\alpha_g}, \tag{3.1}$$

where i is the bubble size group

The net mass source for size group i due to bubble coalescence and break-up can be expressed as the sum of bubble birth rates due to the break-up of larger bubbles from groups $j > i$ to group i and coalescence of smaller bubbles from size groups $j < i$, to group i. Similarly, the net mass source for size group i due to bubble coalescence and break-up is the sum of bubble death rates due to break-up of bubbles from size group i to smaller bubbles in groups $j < i$ and the coalescence of bubbles from size group i with bubbles from any other group to even larger ones which belong to groups $j > i$. The size fraction has been set as boundary condition as well as initial condition in the simulations performed in this thesis. Depending on the superficial velocities of the phases, different size fractions were set for different experimental cases studied in this thesis.

3.7.1 Coalescence and breakup

The birth and death rates are commonly expressed in terms of coalescence and breakup kennels. The phenomenon of fluid particle coalescence and breakup has been the subject of considerable theoretical and experimental attention over the past decades. A variety of

models have been published to determine the coalescence frequency which is made up of physical and empirical models. Some modifications are proposed in more recent work to account for the effect of size ratio between bubbles and eddies and also to consider the existence of bubbles that reduces the free space for bubble movement and causes an increase in the collision frequency.

In this thesis, the breakup model of Luo and Svendsen (1996) which is based on the assumption of bubble binary breakup under isotropic turbulence has been used. The breakup rate was modelled as:

$$\Omega\left(D_j, D_1\right) = 0.923 F_B \left(1-\alpha\right)\left(\frac{\varepsilon}{D_j^2}\right)^{1/3} \int_{\min}^{1} \frac{\left(1+\xi\right)^2}{\xi^{11/3}} \exp\left(-\frac{12 C_f \sigma}{\beta \rho_c \varepsilon D_j^{5/3} \xi^{11/3}}\right) d\xi \tag{3.2}$$

where F_B is a calibration factor to harmonise the mechanism of bubble breakup.

The model of Prince and Blanch, (1990) was used in his thesis to account for the phenomenon of bubble coalescence. The collisions between bubbles may be caused by turbulence, buoyancy or laminar shear. Collision caused by turbulence has been considered in the present study and the coalescence frequency was therefore modelled as:

$$\psi\left(D_i, D_j\right) = F_C \Gamma_{turb}\left(D_i, D_j\right) \lambda\left(D_i, D_j\right) \tag{3.3}$$

where F_C is a calibration factor to harmonise the mechanism of bubble coalescence.

From literature, it has been observed that coalescence and breakup rates are not the same. To account for the difference in the coalescence and breakup rates, researchers have to fine tuned the calibration factors to match their experimental data. Chen et al. (2005),

enhanced the break-up rate by a factor of 10 in their numerical calculations. Olmos et al., (2001) used a calibration factor of 0.075 to enhance the break-up rates. Yamoah (2014), used a coalescence factor of $F_c = 0.05$ and break-up factor of $F_B = 0.2$ to enhance the coalescence and breakup rates. With focus on coalescence phenomena, the Prince and Blanch, (1990) has been implemented in this thesis with modification. Instead of specifying constant value for the coalescence calibration factor, different expressions that take into account the volume fraction of the bubble have been modelled using CFX Expression Language (CEL) (see appendix). Detailed discussion on the importance and role of these models have been presented in Chapter 2 (Section 2.4). Three cases have been investigated to account for the coalescence calibration factor as expressed below.

Case 1

$$F_C = \left(\left[1 - \exp\left(-C \frac{\alpha_{\max}^{1/3} \alpha_g^{1/3}}{\alpha_{\max}^{1/3} - \alpha_g^{1/3}} \right)^6 \right] \times \left[\exp\left(-\left(\frac{\alpha_{\max}^{1/3} - \alpha_g^{1/3}}{\alpha_g^{1/3}} \right)^2 \right) \right] \right) \tag{3.4}$$

where C is an adjustable parameter, depending on the properties of fluid, C=3 used Wu et al and in this thesis work C=3. $\alpha_{\max}$ is the maximum volume fraction and for case 1, $\alpha_{\max}$ = 0.6 (Lehr et al., 2002)

Case 2

$$F_C = \left(\exp\left[-\frac{\alpha_{\max}^{1/3} - \alpha_g^{1/3}}{\alpha_g^{1/3}} \right] \times \exp\left[-\left(\frac{\alpha_{\max}^{1/3} - \alpha_g^{1/3}}{\alpha_g^{1/3}} \right)^2 \right] \right) \tag{3.5}$$

For case 2, $\alpha_{\max}$ = 0.6 (Lehr et al., 2002)

Case 3

$$F_C = \left(\exp\left[-\frac{\alpha_{\max}^{1/3} - \alpha_g^{1/3}}{\alpha_g^{1/3}} \right] \times \left[\frac{\alpha_{\max}}{\alpha_{\max} - \alpha_g} \right] \right) \tag{3.6}$$

For case 3, $\alpha_{\max}$ = 0.8 (Wang et al., 2005a)

In summary, numerical investigations using the MUSIG model has been conducted in this thesis. The coalescence model of Prince and Blanch, (1990) has been modelled with modification by using an expression dependent on the gas volume fraction of the bubbles to account for the coalescence calibration factor. The breakup of larger bubbles into smaller bubbles has been accounted for using the Luo and Svendsen, (1996) model. In the next Chapter, the results of the numerical investigations performed in this thesis is presented and discussed.

Chapter 4

Results and Discussion

This Chapter contains the results and discussion of the numerical simulations presented in Chapter 3. With the purpose of assessing the models used within a wide range of flow scenarios, six different experimental data that represent different combinations of gas and liquid superficial velocities (see Section 3.2) were used. In other to avoid the fine tuning procedure of selecting calibration factors to harmonise the coalescence and breakup effects, a breakup calibration factor of 0.2 was used (Yamoah 2014) and three different expressions from literature have been modelled to account for the coalescence calibration factor. Using this approach, the coalescence model of Prince and Blanch (1990) were modified and the modified (see equation 3.3-3.6) model implemented in ANSYS CFX code. The numerical results of gas volume fraction, interfacial area concentration, Sauter mean bubble diameter, gas velocity and liquid velocity have been compared with the experimental data reported by Monrós et al., (2013) at the axial location of L/D=98.7 (Top Port). The following interfacial force models were set based on recommendations from Yamoah (2014): the Grace drag force (Grace et al., 1976), the Tomiyama lift force (Tomiyama, 1998) with modification of the aspect ratio, Antal et al., (1991) wall lubrication force with coefficients (-0.01 and 0.05), and Lopez de Bertodano (1991) turbulent dispersion force with coefficient 0.5. The bubble induced turbulent model of Sato (1981) was also used. Analysis was carried out to test the modified coalescence model. The results of the analysis for all the six experimental conditions are presented below.

4.1 Interfacial Area Concentration

The numerical results of interfacial area concentration and experimental results are shown in Figure 4.1 below.

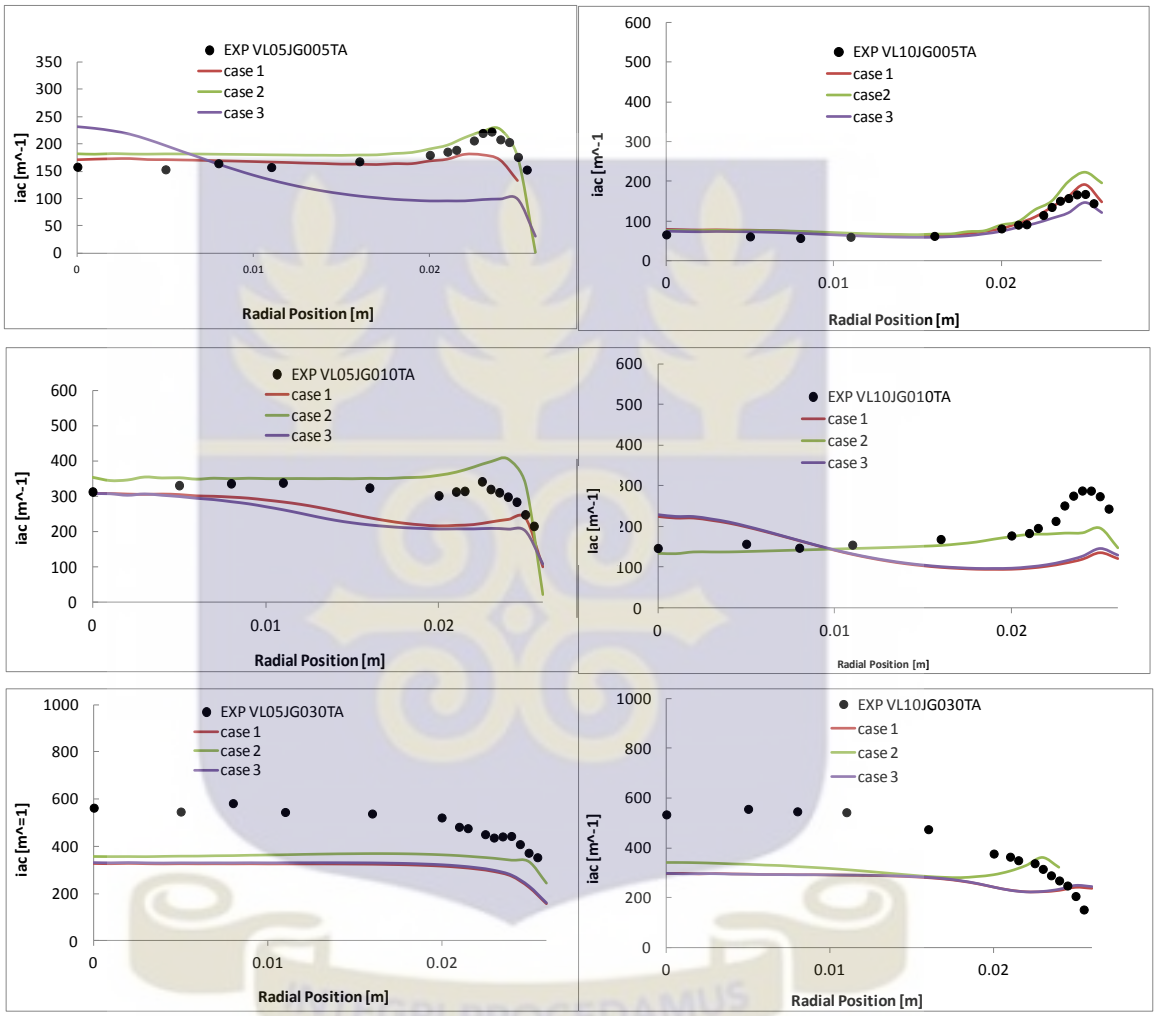

Figure 4.1: Comparison of predicted radial Interfacial Area concentration for case 1, case 2, and case 3.

It is observed from Figure 4.1 that the interfacial area concentration profiles, gives higher values near the wall than at the center of the pipe for both the simulated and the experimental data. For the case labelled VL05JG030TA and VL10JG030TA (see figure

4.1) both simulated and experimental data exhibit a core peak profile. One can also notice that for the experimental condition labelled VL10JG005TA predictions for all the three cases are in good agreement with the experimental data. The reason for the good predictions for this experimental condition could be due to a reasonably good prediction of the bubble diameter and gas volume fraction values together with good combination of interfacial force models. Similar trend is observed for the gas volume fraction and this is because the interfacial area concentration depends not only on the volume fraction of the phase, but also on the bubble size distribution. Again, it is observed that the breakup due to turbulent impact is lower than the absolute ratio of coalescence due to random collision and this happens near the wall. This behaviour leads to low values of the numerical predictions near the wall region for interfacial area concentration, even when the predictions of the gas volume fraction are accurate. This observation is more associated with cases 1 and 3 in almost all the experimental conditions simulated except for VL05JG030TA and VL10JG030TA where all three cases gave low predictions of the interfacial area concentration throughout the pipe domain. From the results obtained from Figure 4.1, it can be said that the modelled expressions for coalescence gave good account of evolution of the bubble size distribution since all the cases generally showed good agreement with the experimental data.

4.2 Gas Volume Fraction

The simulation results of the gas volume fraction profiles are generally in satisfactory agreement with the experimental data as shown in Figure 4.2.

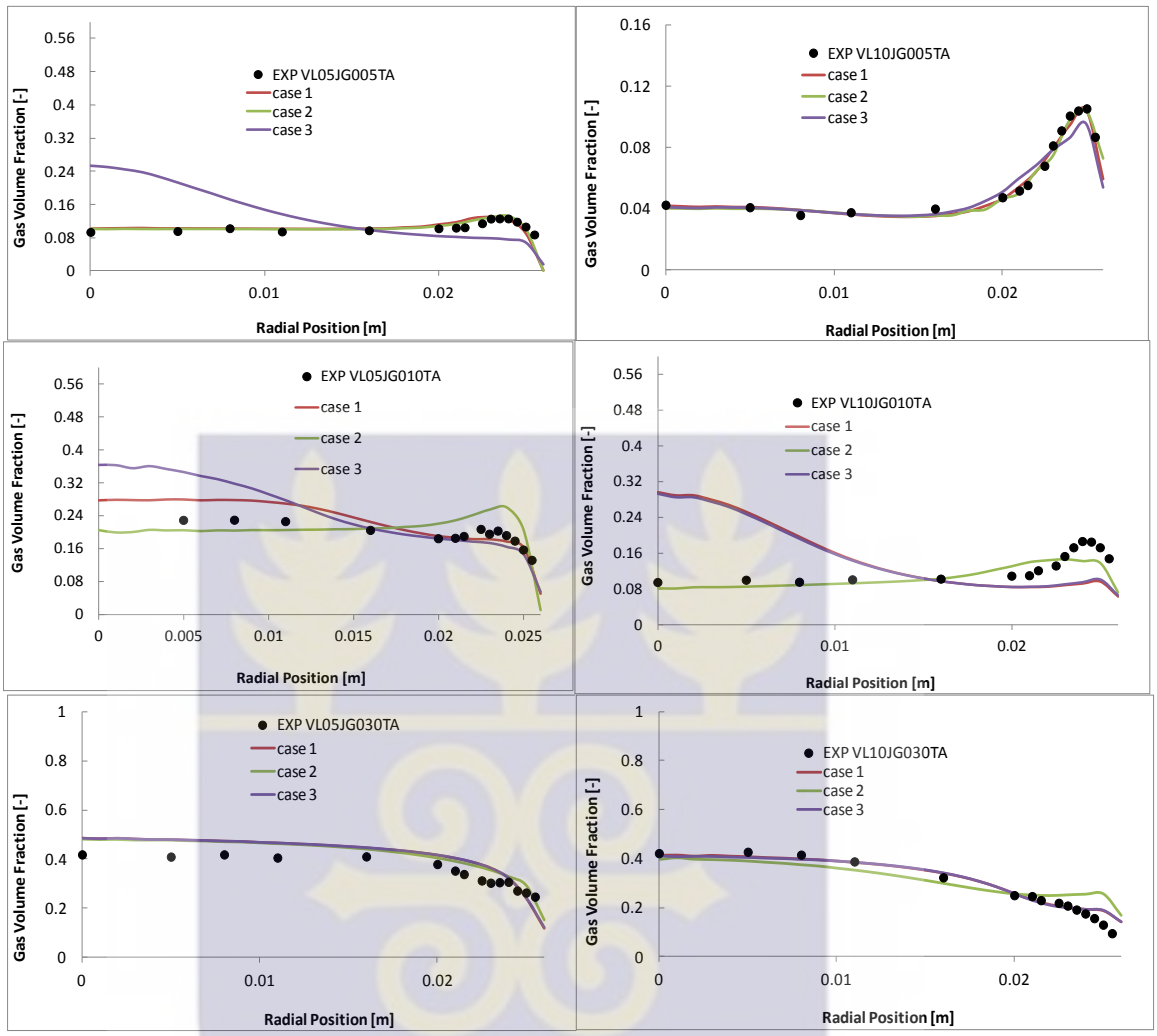

Figure 4.2: Comparison of predicted radial gas volume fraction profile for case 1, case 2, and case 3.

The profile of figure 4.1 shows a characteristic trend with the profile of figure 4.2. This clearly shows that interfacial area concentration depends on the gas volume fraction. Again for the fact that the interfacial area and gas volume fraction are measured differently and showing a relative good prediction of the radial profiles of the interfacial area concentration provides a valuable test of the model prediction from the MUSIG model. For cases labelled VL05JG005TA, VL05JG010TA, and VL10JG010TA show

wall peak profile. The wall peak is mainly due to the positive lift force pushing the small bubbles towards the wall of the pipe. The case labelled VL05JG030TA and VL10JG030TA show a core peak profile. The core peak behaviour is mainly due to large or deformed bubbles experiencing negative lift force which pushes the bubbles to the core of the pipe. The profile of Case 2 gives better prediction with the experimental data. In the case labelled VL10JG005TA, predicted correctly with the experimental data depicting the wall peak behavior. In general one can say that the profiles of all the cases are in good agreement with the experimental data. For cases labelled VL05JG010TA and VL010JG010TA, the profile of Case 1 and Case 3 show slight difference with the experimental data. This is so because, the gas volume fraction at the core and at the wall were under/over-predicted respectively by all models. From the results obtained, one can say that the MUSIG model used is able to account correctly the evolution of bubble in the vertical pipe.

4.3 Sauter mean bubble diameter

The numerical results of sauter mean bubble diameter is in good agreement with the experimental data. The case labelled VL05JG005TA, VL05JG010TA, VL10JG005TA and VL10JG010TA show wall peak profile.

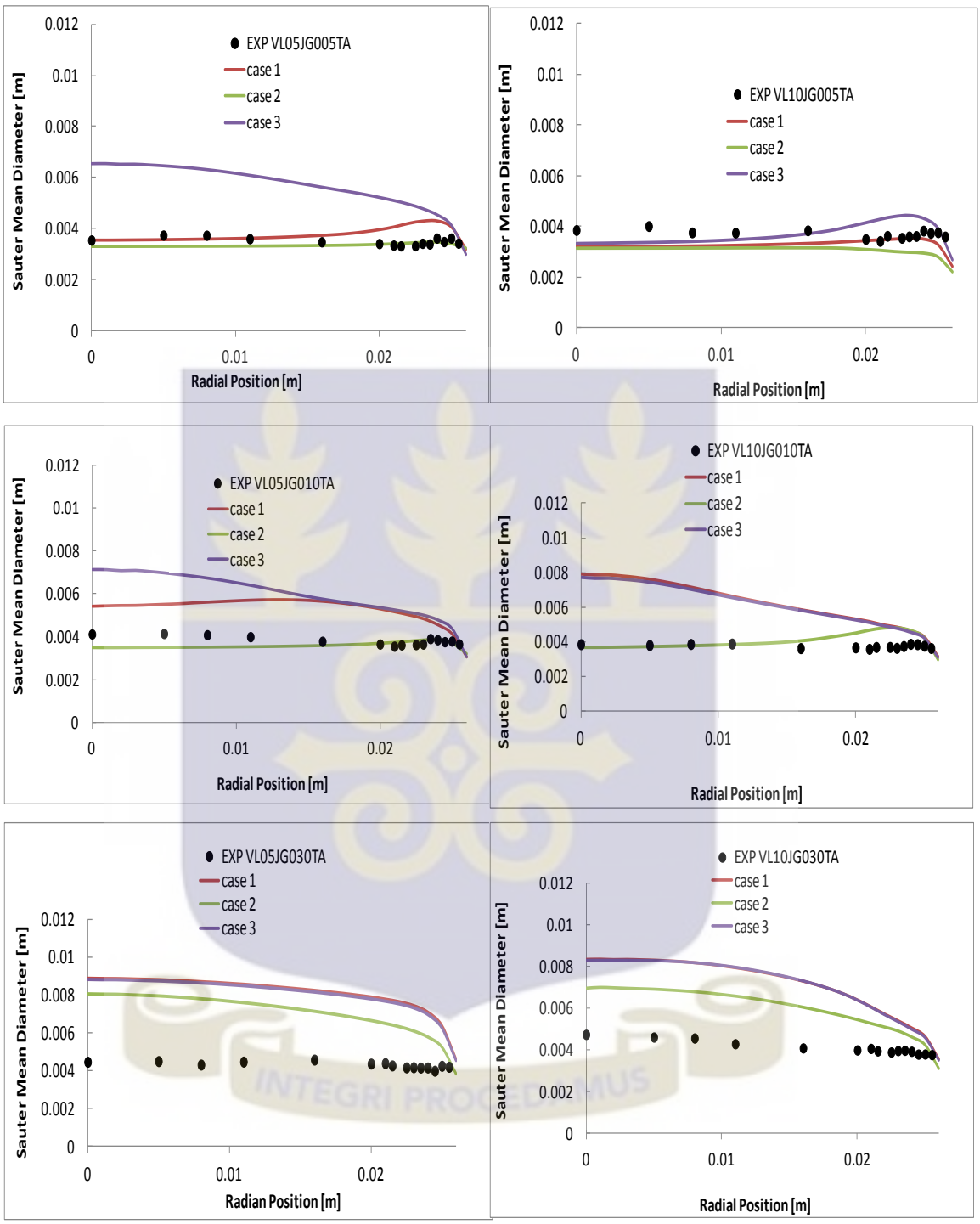

Figure 4.3: Comparison of predicted radial sauter mean bubble diameter profile for case 1, case 2 and case 3.

Here it is observed that both the simulated profile and the experimental profiles are almost uniform along the radial direction except near the wall. Close to the wall sauter bubble diameter tends to reduce. This fact can be linked to high gradient at the wall region. The phenomenon can also be attributed to the fact that the sauter mean bubble diameter increases with increasing superficial gas velocity and vice versa. The profile of Case 2 gives satisfactory agreement with the experimental data when compared with Case 1 and Case 3. The potential tendency of small bubbles migrating towards the wall provides considerable possibility for highly concentrated bubbles to merge together to form slightly larger bubbles, hence a higher peak is observed at the wall region.

For the cases labelled VL05JG030TA and VL10JG030TA, they depict core peak profile. In cases labelled VL05JG005TA and VL10JG005TA, one can say that all the cases were predicted accurately with experimental data.

The simulation results obtained for the sauter mean bubble diameter shows that all the models captured correctly the evolution of the bubble size distribution.

4.4 Gas Velocity Profile

The numerical simulation for gas velocity profile has been shown in Figure 4.4 for all the three cases and the result is in good agreement with the experimental data. It is evident that for experimental conditions VL05JG030TA, VL10J050TA and VL10JG030TA there is no appreciable differences between the results obtained by the three cases. However, one could notice differences between the results of the three cases for experimental conditions VL05JG005TA, VL05JG010TA and VL10JG010TA. For the experimental condition VL05JG030TA, all the three cases predicted lower than the experimental value.

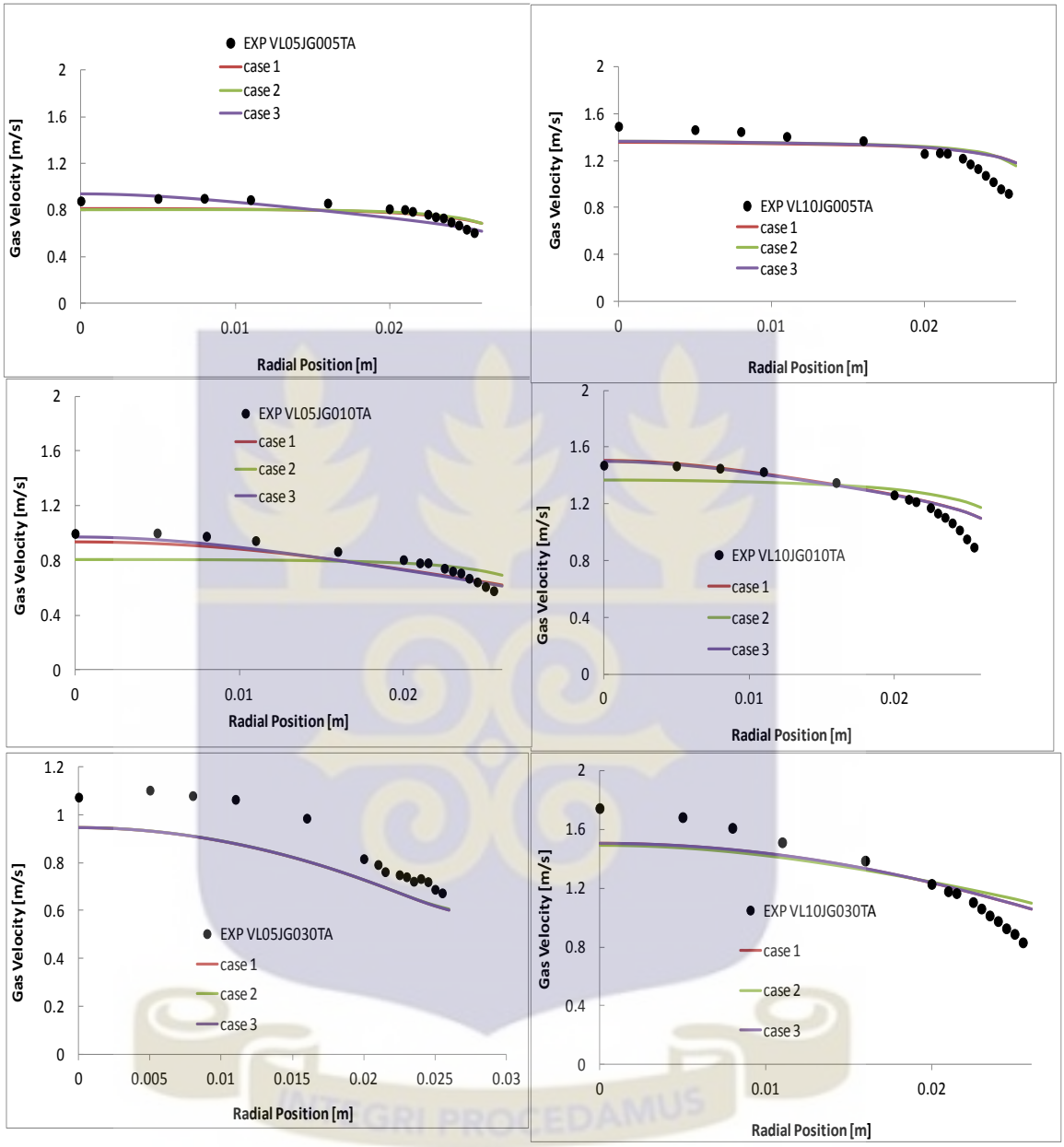

Figure 4.4: Comparison of predicted radial gas velocity profile for case 1, case 2, and case 3

From Figure 4.4, it can be concluded that case 1and 3 were able to predict the experimental gas velocity profile much better than case 2 in most of the experimental

conditions. Also of interest to note is that for the experimental conditions VL10JG005TA, VL10JG010TA and VL10JG030TA, the simulated gas velocity is over predicted close to the wall resulting in a flattened profile at the core. This phenomenon could be due to under sampling of the liquid flow field in the vicinity of the wall causing the velocity profile not to fall smoothly to zero.

4.5 Liquid Velocity

Figure 4.5 shows the measured and predicted radial profiles of the liquid velocity for all the cases. It is evident that there are significant differences between the predictions for the three cases except for experimental condition VL05JG030TA. Unlike the gas velocity profile, case 2 were able to reasonably predict the liquid velocity profile much better than cases 1 and 3. However, in generally both case predictions reasonably agree well with the experimental data. It should be noted that the curves for experimental condition VL10JG030TA are not shown as there no experimental data available for comparison.

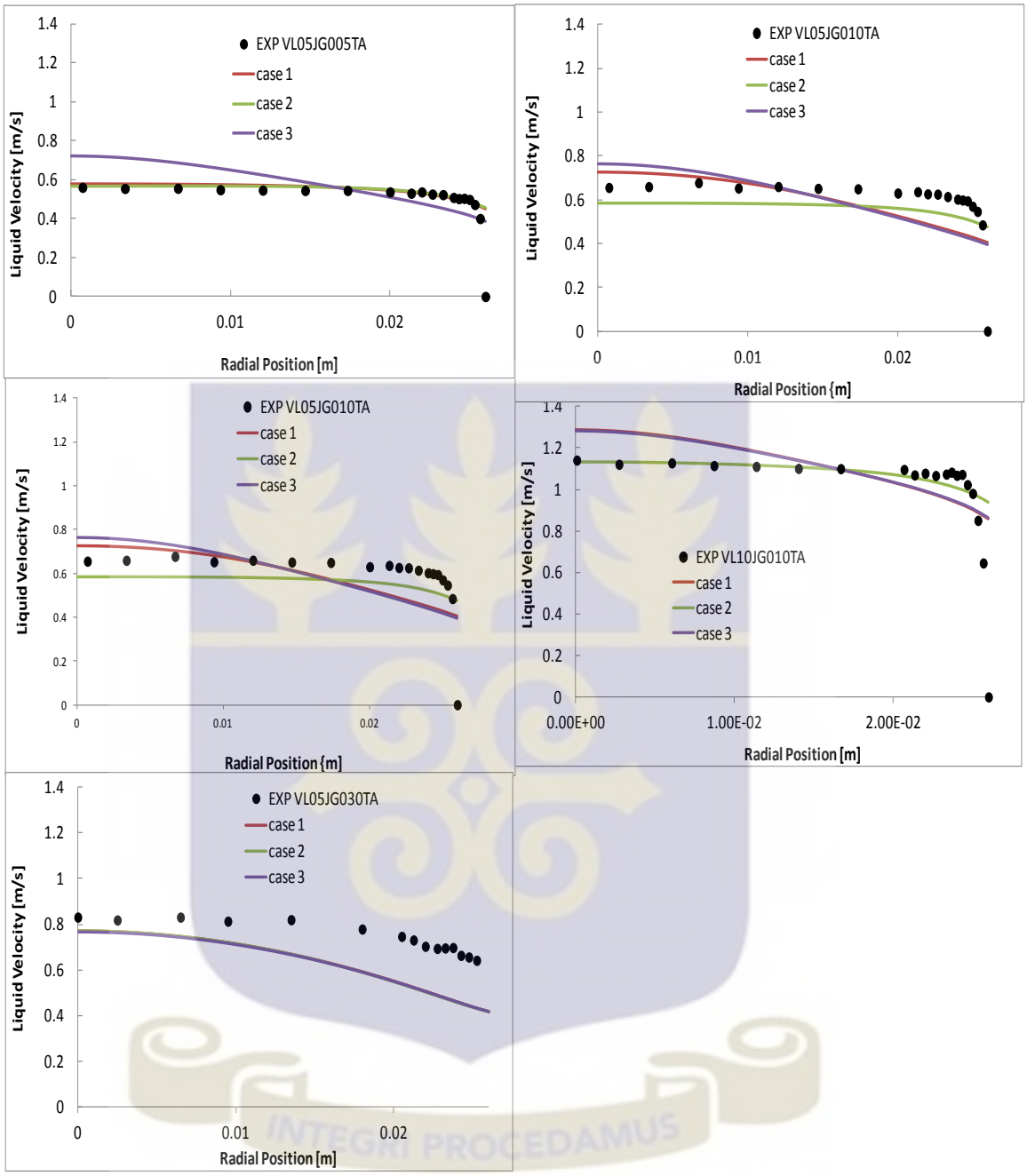

Figure 4.5: comparison of predicted radial profile liquid velocity profile for case 1, case 2 and case 3.

4.6 Comparison of results with Yamoah, (2014)

In this Section, results obtained from this thesis has been compared with selected results by Yamoah (2014). It is evident from the results as presented in Section 4.1 to 4.5 that overall the model labelled as case 2 presented the best results in most of the experimental conditions. Therefore, in order to further test the capability of the model, case2 was verified with a selected result by Yamoah (2014) that has the same interfacial force settings, boundary conditions and grid as was used in this thesis. The comparison of the numerical results with the experimental data showed good agreements (Yamoah, 2014). However, in the case of Yamoah (2014) a constant value for the coalescence and breakup calibration factors were respectively set at $F_C = 0.05$ and $F_B = 0.2$. In this thesis $F_B = 0.2$ was maintained whereas F_C was modelled. Thus, the purpose here is to verify the new approach used in this thesis. Thus, numerical results of gas volume fraction, interfacial area concentration and Sauter mean bubble diameter obtained using case 2 and Yamoah (2014) has been compared and presented below.

In Figure 4.6, profiles of simulated and measured radial gas volume fraction is presented. Evidently it can be observed that satisfactory results have been obtained for Yamoah (2014) and case 2 of this thesis.For the experimental condition labelled as VL05JG005TA, VL10JG005TA, and VL10JG010TA no significant differences could be observed between the two numerical approaches (that is Yamoah, 2014 and case 2) and the predictions were satisfactorily in agreement with the experimental data.

However, for the experimental condition labelled as VL05JG010TA, VL05JG030TA and VL10JG030TA, significant differences could be observed between the numerical and the experimental results. Generally in all three experimental conditions listed above, case

2 gave relatively good predictions except for the conditions labelled VL05JG030TA where Yamoah (2014) was able to predict the core profile more satisfactorily than case 2.

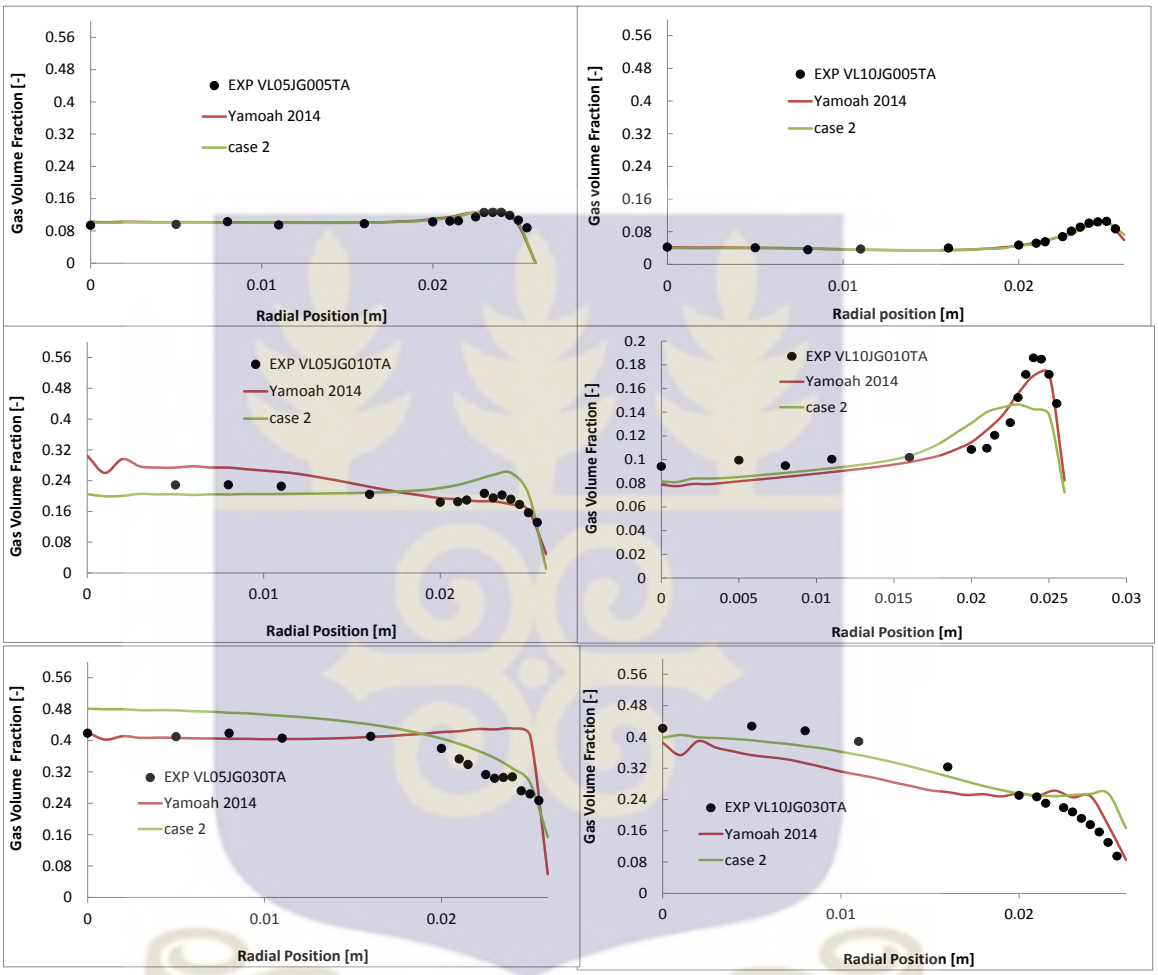

Figure 4.6: Comparison of predicted radial gas volume fraction profile for Yamoah 2014 and Case 2.

The measured and predicted radial profiles for interfacial area concentration has been shown in Figure 4.7 for both Yamoah (2014) and case 2. From the Figure it can be observed that the simulation results of the interfacial area concentration for Yamoah (2014) and case 2 are generally in good agreement with experimental data. One can

noticed that the profle and predicted trend of interfacial area concentration shows similarity as that of the gas volume fraction profile.

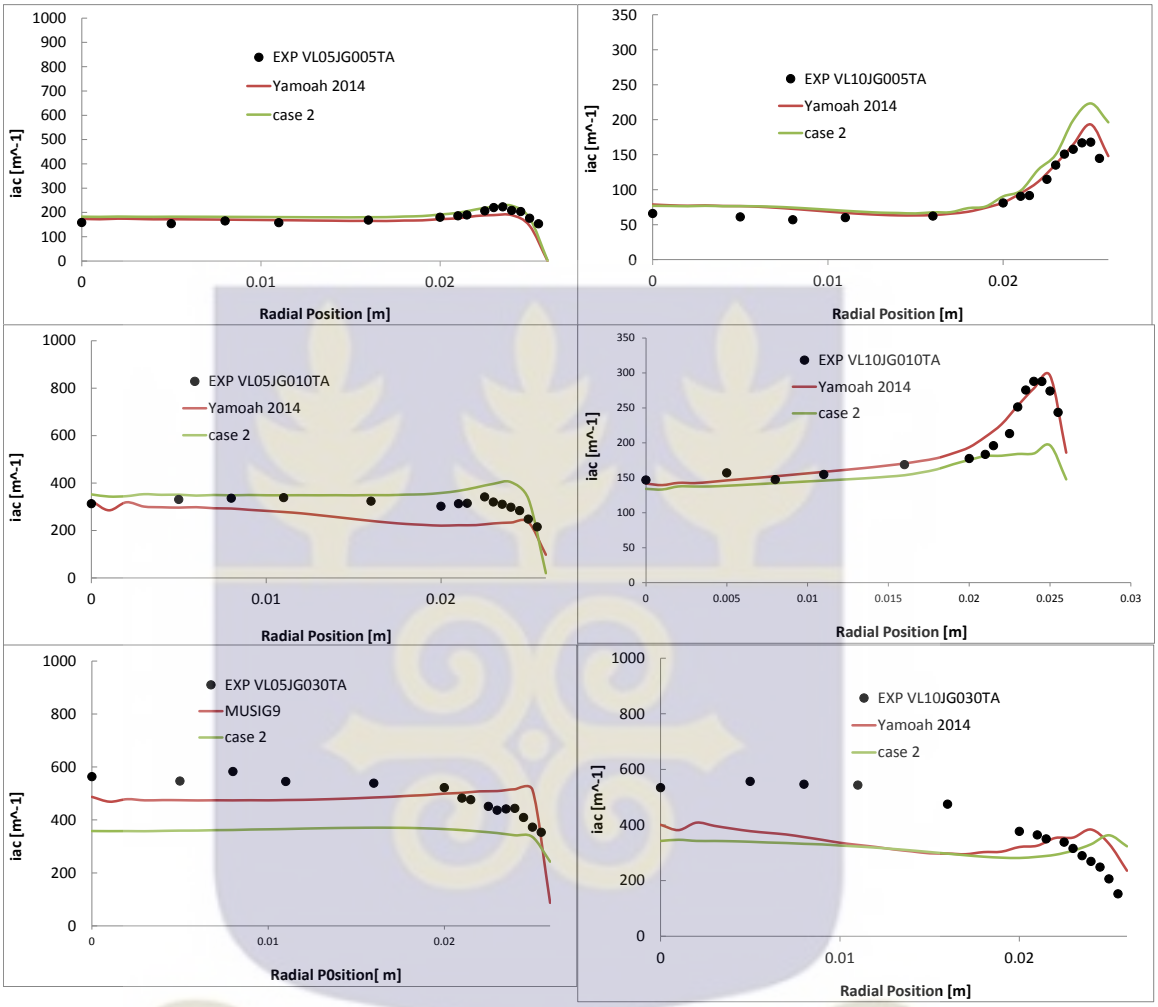

Figure 4.7: Comparison of prediction radial interfacial area concentration profile for Yamoah 2014 and case 2

This is so because the interfacial area concentration depends on the volume fraction and also the bubble size distribution. It can however be observed that unlike the gas volume fraction profile, the IAC was slightly better predicted by Yamoh (2014) than case 2.

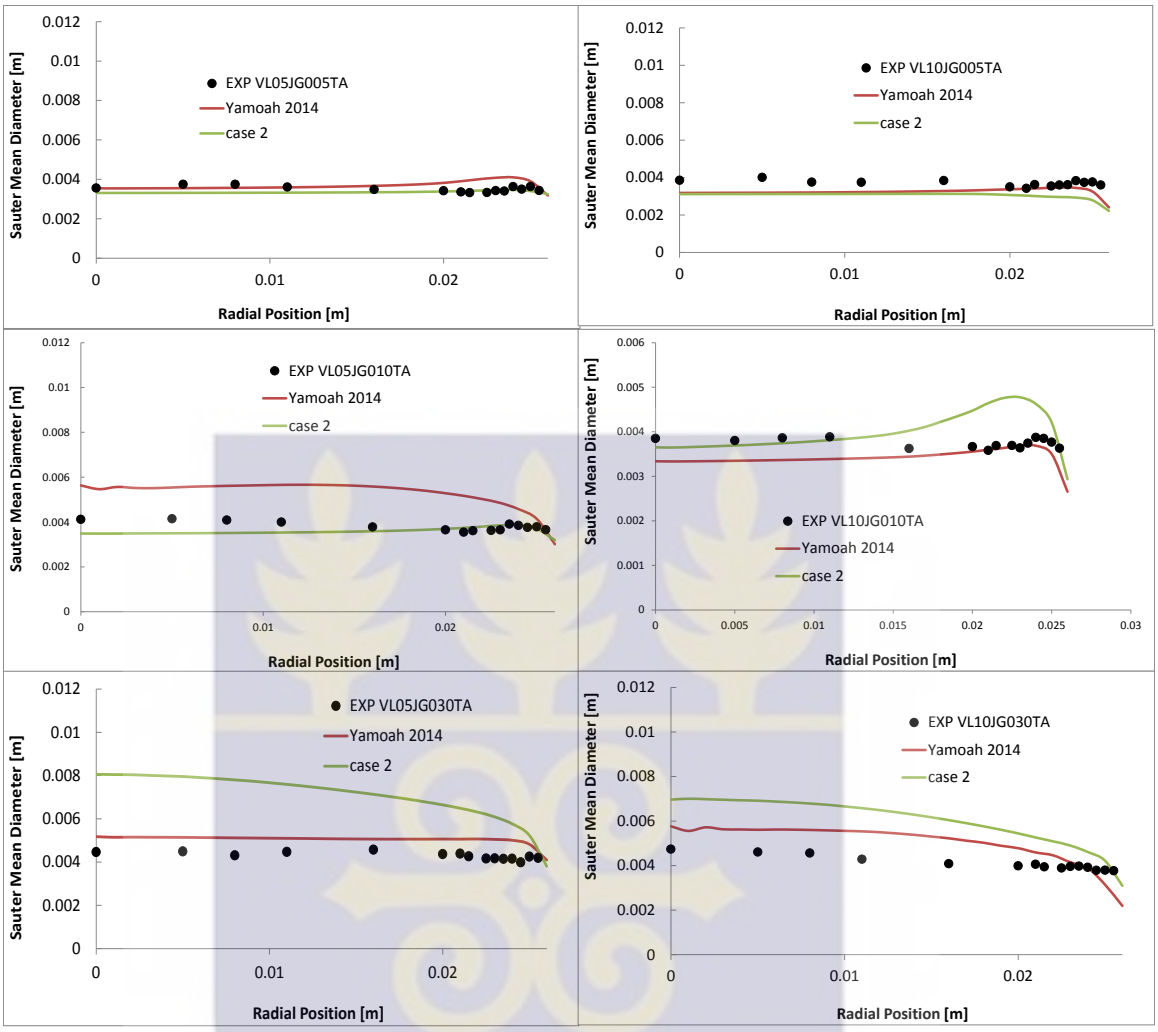

Figure 4.8: Comparison of predicted radial sauter mean diameter profile forYamoah 2014 and case 2.

Looking at the good prediction of the numerical and experimental results, and the fact that the interfacial area concentration is measured differently from the gas volume fraction and the two having similar profile trends shows that the MUSIG model correctly predicted the evoluton of the bubble sizes.

The comparison of the result of case 2 with Yamoah (2014) for the Sauter mean bubble diameter has been shown in Figure 4.8. From the Figure, one can notice that there are

significant differences between the two approaches expecially for experimental conditions VL05JG010TA, VL05JG030TA, VL10JG010TA and VL10JG030TA. For example while case 2 was able to reasonably predict the experimental data better than Yamoah (2014) for experimental condition VL05JG010TA , Yamoah (2014) did predict better than case 2 for experimental condition VL05JG030TA . The ability to better predict the Sauter mean bubble diameter directly influences how well the interfacial area concentration can be predicted. It should also be noted that the interfacial area concentration does not only depend on the Sauter mean bubble diameter but also on the volume fracton of the disperse phase. Overall both case 2 and Yamoah (2014) predicted reasonably well the Sauter mean bubble diameter for all the experimental conditions simulated in this thesis.

In conclusion, numerical results of the evolution of bubble size distribution using the MUSIG model has been presented. Three different modifications (labelled as case 1, case 2 and case 3) have been investigated and compared with each other in this thesis. The predicted local radial distributions of gas volume fraction, interfacial area concentration, Sauter mean bubble diameter, gas velocity and liquid velocity have been validated against the experimental data reported by Monrós et al. (2013). Generally, both cases were able to reasonably predict the experimental data. Overall case 2 turns out to be the best among the other cases. Subsequently case 2 was verified with a selected result by Yamoah (2014) that has the same numerical settings. In general, the verification showed good agreement with Yamoah (2014).

Chapter 5

Conclusion and Recommendations

5.1 Conclusion

In this thesis, numerical investigation of the performance of the homogeneous MUSIG model in tracking the internal phase distribution of gas-liquid two-phase bubbly flow in a vertical pipe has been presented. Particularly, the research focus has been centered on better understanding of the population balance modelling and the effects of the coalescence and breakup phenomenon. The coalescence model of Prince and Blanch (1990) has been used in this thesis with modification. For the effect of breakup, the model of Luo and Svendsen (1996) has been used. The radial separation of small and large bubbles could be shown as an essential phenomenon, which must be considered by an adequate simulation. Therefore, bubbles have been distributed into 10 diameter classes ranging from 1 mm to 10mm based on investigation of sensitivity analysis of number of size groups. There are two major contributions from this study: (1) a modification of the coalescence model of Prince and Blanch (1990) to account for the imbalance between coalescence and breakup phenomenon; and (2) the population balance approach with implementation of the modified model into ANSYS CFX code using CFX Expression Language (CEL).

The modification resulted in a new model which is not experimentally dependent. This means that the model can be applied to all experimental conditions as against the practice whereby various researches specify constant calibration factors to account for the imbalance between the coalescence and breakup models. Using the later approach,

various researchers come up with different calibration factors to match their experimental data. Three different modifications has been investigated and compared with each other in this study.

With the aim of assessing the model performance, the predicted local radial distributions of gas volume fraction, interfacial area concentration, Sauter mean bubble diameter, gas velocity and liquid velocity have been validated against the experimental data reported by Monrós et al. (2013). In general, the comparison has shown that the MUSIG model yielded satisfactory agreement with the experimental data. The transition of phase distribution of the gas from wall peaking to core peaking is reasonably captured by most of the models. The encouraging results obtained clearly show the capability of the models used in capturing the evolution of the bubble size. . The predictions of the interfacial area concentration for all the cases generally showed good agreement with the experimental data and this provides a valuable test of the models (cases). The IAC characteristically show trends that are similar to the gas volume fraction profiles. The observed agreement with the gas volume fraction profiles indicates a level of confidence in the interfacial force models used. On the other hand, the agreement seen on the interfacial area concentration indicates that the birth and death processes modelled (that is the new models implemented in this study) are reasonably adequate to describe the bubble dynamics.

Similar conclusions can be said about the numerical predictions of Sauter mean bubble diameter, gas and liquid velocity where also notably satisfying agreement was obtained between the predicted and experimental data.

Overall, the comparison shows that the model labelled as Case 2 presented the best results in most of the experimental conditions. In order to further test the capability of the model, case2 was verified with the results of Yamoah (2014) where the conditions were the same except that in Yamoah (2014) a constant calibration factor of 0.05 was used for the coalescence model. The comparison shows generally reasonable agreement between the two approaches. For the specific case of core peaking gas volume fraction profiles, the model presented in this study gave a relatively better prediction compared to the approach use by Yamoah (2014)

5.2 Recommendations

Notwithstanding the reasonable agreement between the simulated and experimental results, noticeable discrepancies in simulating bimodal bubble size distributions were found revealing the possible imperfection of existing coalescence and breakup kernels. Most of the existing bubble mechanistic models were developed for bubbly flow regime. Directly adopting these kernels to other flow regimes could nonetheless introduce significant error with the calculations Therefore there is the need to include additional bubble mechanisms into the population balance model in order to capture all the essential physical processes occurring in gas-liquid flows. Furthermore the homogeneous MUSIG model could be extended to the inhomogeneous MUSIG model. The inhomogeneous MUSIG model uses different momentum equations to describe individual velocity of each bubble size group.

References

ANSYS CFX Solver Theory Guide (2011), 14th release, ANSYS Inc., Canonsburg, Pennsylvania

ANSYS CFX, (2012). User Manuel, Release 14.5, ANSYS In.

Alexopoulos, A. H., D. Maggioris and C. Kipaurissides, (2002). "CFD Analysis of Turbulence Non-Homogeneity in Mixing Vessels: A Two-Compartment Model", Chem. Eng. Sci. 57, 1735-1752 (2002).

Antal S.p., Lahey Jr R. T., Flaherty J.E., (1991), "Analysis of phase distribution in fully developed laminar bubbly two-phase flow". International Journal of Multiphase Flow, 17, 635.

Burns, A.D., Frank, T., Hamill, I., Shi, J. (2004). The Favre averaged drag model for turbulence dispersion in Eulerian multi-phase flows. In: Proc. 5th Int. Conf. On multiphase flow, ICMF2004, Yokohama, Japan, 2004.

Chaded, J., V. Roig and L. Masbernat, (2003) "Eulerian-Eulerian Two-Fluid Model for Turbulent Gas-Liquid Bubbly Flow", Int. J. Multiphase Flow 29, 23-49.

Chen, P., Sanyal, J., Dudukovic, M.P., (2005). Numerical simulation of bubble columns flows: effect of different breakup and coalescence closures. Chem. Eng. Sci., 60,1085-1101.

Chesters, A.K., (1991). The modelling of coalescence processes in fluid-liquid dispersions: a review of current understanding. Chemical Engineering Research and Design: transactions of institution of Chemical Engineering: Part A 69, 259-270.

Chesters, A. K., Hofman, G., (1982). Bubble coalescence in pure liquids. Applied Scientific Research 38, 353-361.

Cheung S.C.P., Yeoh G.H., Tu J.Y (2009a), "Direct Quadrature Method of Moments for Isothermal bubble flows" Journal of Computational Multiphase Flows, 1(2),161.

Cheung, S.C.P, Yeoh, G.H., Tu, J.Y., (2007a). On the modelling of population Balance in Isothermal Vertical Bubbly Flows- Average Bubble Number Density Approach. Chem. Eng. Process. 46 (8), 742-756.

Colin, C. (2004). Turbulence and Shear-Induced Coalescence in Gas-Liquid pipe Flows. In: Fifth International Conference on Multiphase Flow, ICMFO4, Yokohama, Japan, May 30-June 4

Cong Li, (2011). Numerical Study of Isothermal Gas-Liquid Two-phase Bubbly Flow. PhD Dissertation. Royal Melbourne Institute of Technology (RMIT) University.

Coulaloglou, C, A., (1975). Despersed phase interactions in an Agitated Flow Vessel. Ph.D. Dissertation, Illinos Institute of Technology, Chicago.

Coulaloglou, C. A., Tavlarides, L. L., (1977). Description of interaction processes in agitated liquid-liquid dispersions. Chemical Engineering Science 32, 1289-1297.

Crowe, C., Sommerfeld, M., Tsuji, Y., (1998). Multiphase Flows with droplets and Particles. CRC Press, Boca Raton.

Das, P.K., Kumar, R., (1987). Coalescence of drops I stirred dispersion. A white noise model for coalescence. Chemical Engineering Science 42, 213-220.

Debry E., Sportisse B., Jourdain B. A (2003). Stochastic approach for the Numerical Simulation of the General equation for Aerosols. Journal of Computational Physics, 2003, 184, 649-669.

Deckwer, Wolf-Dieter, Youssef Louisi, Ahmed Zaidi and Milos Ralek (1980). "Hydrodynamic Properties of the Fischer-Tropsch Slurry Process." Industrial & Engineering Chemistry Process Design and Development 19(4): 699-708.

Doubliez, L., (1991). The drainage and rapture of a non-foaming liquid film formed upon bubble impact with a free surface. International Journal of Multiphase Flow 17, 783-803.

Domiovskii E,R., Lushnikov A.A., Piskunov V.N (1979). A Monte Carlo Simulation of coagulation processes. Izvestigya Akademii Nauk SSSR, Fizika Atmosfery I Okeana, 1979, 15, 194-201.

Duineveld, P.C., (1994). Bouncing and coalescence of two bubbles in water. Ph.D. Dissertation, University of Twentte, the Netherlands.

Drew, D. A., Lahey Jr., R.T. (1987). The virtual mass and lift force on a sphere in rotating and straining inviscid flow. Int. Journal Multiphase Flow, v. 13, n. 1, pp. 113-121.

Ervin, E.A., Tryggvason, G., (1997). The rise of bubbles in a vertical shear flow. Journal of Fluids Engineering 119, 443-449.

Friedlander S. K. (2000). "Smoke, dust, and haze: foundationals of aerosol dynamics" (2nd Edition), Ofor university Press.

Fredrickson A. G., Ramkrishna D., Tsuchiya H.M., (1967), "Statistics and dynamics of prokaryotic cell population". Mathematical Bioscience, 1, 327.

Frenklach M. (2002). Method of Moments with Interpolative closure. Chemical Engineering Science, 57, 2229-2239.

Grace, J. R., Wairegi, T. and Nguyen, T.H. (1976). Shapes and velocities of single drops and bubbles moving freely through immiscible liquids. Trans. Instn Chem. Engr 54,167-173.

Grevskott, S., Sannaes, B. H., Dudkovic, M.P., Hjarbo, K. W., Svendsen, H.F., (1996). Liquid circulation, bubble size distributions, and solids movement in two and three-phase bubble columns. Chem. Eng. Sci. 51 (10), 1713.

Hewitt G.F. (2008). Multiphase flow in the energy industries. Journal of Engineering Thermophysics, 17, pp. 12-23

Hibiki, T. and Ishii, M., (2000a). One-group interfacial area transport of bubbly flows in vertical round tubes. International Journal of Heat and Mass Transfer 43, 2711-2726.

Hibiki, T. and Ishii, M., (2000b). Two-group interfacial area transport equations at bubbly-to-slug flow transition. Nuclear Engineering and design 202(1), 39-76.

Hibiki T., Ishii M. (2007). "Lift force in bubbly flow systems". Chemical Engineering Science, 62, 6457.

Hidy G. M., and Broke J. R., (1970). "The dynamics of aerocolloidal system", Trans. American Nucl. Soci, 19, 408.

Howarth, W.J., (1964). Coalescence of drops in turbulent flow field. Chemical Engineering Science 19, 33-38.

Hulburt H. M., Katz S., (1964). Some problems in particle technology: A statistical mechanical formulation. Chemical Engineering Science, 19, 55-574.

Ishii, M. and (1975). Thermo-fluid dynamic theory of two-phase flow. Paris, Eyrolles.

Ishii, M. and T. Hibiki (2006). Thermo-Fluid Dynamics of Two-phase flow. New York, Springer.

Jones, W.P. and B.E Launder, (1973). "The prediction of low-Renolds-number phenomena with a two-equation model of turbulence", Int. J. Heat Mass Trans. 16, 1119-1130.

Kashiwa B A. and W. B. VanderHeyden., An Extended K-Epsilon (1998). Turbulence Model for Multiphase Flow, "Thirteenth U.S. National Congress of Applied Mechanics", University of Florida, Gainesville, FL.

Kennard, E. H. (1938). Kinetic theory of gases: with an introduction to statistical mechanics, McGraw-Hill.

Kocamustafaogullari G, and Ishii M., (1995). Foundation of the interfacial area transport equation and its closure relations. International Journal of Heat and Mass Transfer, 38,481.

Krepper, E., Beyer, M., Frank, T., Lucas, D., Prasser, H.M., (2007). Application of a population balance approach for polydispersed bubble flow. 6th International Conference on Multiphase Flow, ICMF06, 09.-13.07.2007, Leipzig, Germany, Poster NoPS6_6.

Krepper, E., Prasser, H.M., (2000). Measurements and CFX simulations of a bubbly flow in a vertical pipes. AMIFESF Workshop, Computing Methods in two-phase flow.

Krepper, E., Lucas, D., Prasser, H.M., (2005). On the modelling of bubbly flow in vertical pipes. Nucl. Eng. Des.235 (5), 597-611. Kuboi, R., et al., (1972). Collision and coalescence of dispersed drops in turbulent liquid flow. Journal of Chemical Engineering of Janpan 5,423-424.

Kumar, S. and D. Ramkrishna (1996a). "On the solution of population balance equations by discretization. 1. A moving pivot technique." Chemical Engineering Science 51(8): 1333-1342.

Kumar, S. and D. Ramkrishna (1996b). "On the solution of population balance equations by discretization. 1. A fixed pivot technique. "Chemical Engineering Science 51 (8) 1311-1332.

Lasheras J. C., Eastwood C. Martinez Bazan C. and Montanes J.L., (2002). A review of statistical models for the break-up of an immiscible fluid immersed into a fully developed turbulent flow. International Journal of Multiphase Flow, 28, 247-278.

Lee, C.H., (1987a). Bubble breakup and coalescence in turbulent gas-liquid dispersions. Chemical Engineering Communication 56, 65-84.

Lehr F.Millies M., and Mewes D., (2002). Bubble-size distributions and flow fields in bubble columns. AIChE Journal, vol.48, no.11, pp.2426-2443.

Lehr, F., Mewes, D., (1999). A transport equation for the interfacial area density applied to bubble columns. Chemical Engineering Science 56, 11, pp.2426-2443.

Levich, V.G., 1962, Physicochemical Hydrodynamics. Prentice Hall, Engiewood Cliffs, NJ.

Liao, Y., Lucas, D., (2009). A literature review of theoretical models for drop and bubble breakup in turbulent dispersions. Chemical Engineering Science, 64, pp.3389-3406.

Liao, Y., Lucas, D., (2010). A literature review on mechanisms and models for the coalescence process of fluid particles. Chemical Engineering Science, 65, pp-2851-2864

Liao Y., Lucas D., Krepper E., Schmidtke M., (2011). Development of generalized coalescence and breakup closure for inhomogeneous MUSIG model, Nuclear Engineering, Design, 241, 1024-1033.

Liffman, Kurt (1992). "a direct simulation Monte Carlo method for cluster coagulation."Journal of Computation Physics 100(1): 116-127.

Lilunnahar, Deju (2014). Population Balance Modelling of Gas-Liquid Bubbly: Capturing Coalescence and Breakup Processes. PhD dissertation. Engineering and Health RMIT University.

Lo, s., (1996). Application of Population Balance to CFX Modelling of Bubbly Flow via the MUSIG model, AEA Technology, AEAT-1096.

Lopez de Bertodano, M., (1991). Turbulent Bubbly flow in a Triangular Duct, Ph.D Thesis, Rensselaer Polytechnic Institute, Troy New York.

Lopez de Bertodano, M., Lahey Jr., R.T., and Jones, O.C (1994b). Development of a k-e model for bubbly two-phase flow, Trans. ASME J. Fluids Eng, Vol. 116, p. 128.

Lopez de Bertodano, M., Lahey Jr., R.T., and Jones, O.C (1994b). Phase distribution in bubble two-phase flow in vertical ducts, Int. J. Multiphase Flow, Vol. 20, p. 805.

Lopez de Bertodano, M., (1998). Two fluid model for two-phase turbulent jet, Nucl. Eng. Des. Vol 179, p. 65.

Lucas D., Krepper E., Prasser H.M. Development of co-current air-water flow in vertical pipe. International Journal of Multiphase flow, 2005, 31, 1304-1328.

Lucas, D., Krepper, E., Prasser, H.-M. Manera, A. (2006). Investigations on the stability of the flow characteristics in bubble column, Chemical Engineering Technology, vol. 29, pp. 1066-1072.

Luo H., Svendsen H., (1996). "Theoretical model for drop and bubble breakup in turbulent dispersions". AIChE Journal, 42, 1225.

Luo H., (1993). "Coalescence, breakup, and liquid circulation in bubble column reactors". Ph.D Dissertation, the Norwegian Institute of Technology, Trondheim.

Magnaudet, J., Legendre, D., (1997). Some aspects of the lift force on a spherical bubble. Appl. Sci. Res. 58 (1-4), 441-461.

Magnaudet, J., Eames, I., (2000). The motion of high-Reynolds-number bubbles in inhomogeneous flows. Annual. Rev. Fluid Mech. 32, 659-708.

Maisel, Arkadi, F. Einar Kruis and Heinz Fissan (2004). "Direct simulation Monte Carlo for simultaneous nucleation, coagulation, and surface growth in dispersed systems."

Chemical Engineering Science 59(11): 2231-2239

Martinez-Bazan, C., J. L. Montanes and J. C. Lasheras (1999a). "On the breakup of an air bubble injected into a fully developed turbulent flow. Part 1. Breakup frequency. "Journal of fluid mechanics 401: 157-182.

Martinez-Bazan, C., J. L. Montanes and J. C. Lasheras (1999b). "On the breakup of an air bubble injected into a fully developed turbulent flow. Part 2. Size PDF of the resulting daughter bubbles. Journal of Fluid Mechanics 401: 183-207.

McCoy B.J., Madras G., (2003), "Analytic Solution for a population balance equation with aggregation and fragmentation". Chemical Engineering Science, 58, 3049.

Menter, F.R., (1994). Two-equation eddy-viscosity turbulence models for engineering applications". AIAAJ, 32, 1598. 32, 1598-1605.

Monrós-Andreu G., Chiva S., Martínez-Cuenca R., Torró S., Juliá J.E., Hernández L., Mondragon R., (2013). Water temperature effect on upward air-water flow in a vertical pipe. Local measurements database using four-sensor conductivity probes and LDA. EPJ Web of conference 45,01105.

Moraga, J.F., Larreteguy, A.E., Drew, D.A., and Lahey, R,T., (2003). Assessment of turbulent dispersion models bubbly flows in the low Stokes number limit. Int. J. Multiphase Flow, 29, p. 655.

Olmos, E., Gentric, C., Vial, Ch., Wild,G. and Midoux N., (2001). Numerical simulation of multiphase flow in bubble column reactors. Influence of bubble coalescence and break-up. Chemical Engineering Science, vol. 56, (21-22), 6359-6365.

Pandis S.N., Seinfeld J.H. (1998) Atmospheric chemistry and physics: From air pollution to climate change. New York: wiley.

Park, J.Y., Blair, L.M., (1975). The effect of coalescence on drop size distribution in an agitated Liquid-Liquid dispersion. Chemical Engineering Science 30, 1057-1064.

Prince, M. J., Blanch, H. W., (1990). Bubble coalescence and break-up in air-sparged bubble-columns. AIChE J.36 (10), 1485-1499.

Ramkrishna D. (1979), statical models of cell population, In: Ghose TK, Fiechter A, Blakebrough N (Eds)", Advances in Biochemical Engineering, vol. 11, Berlin: springer.

Ramkrishna D., (1985), "The status of population balances". Reviews in chemical engineering, 3, 49.

Ramkrishna D., (2000), "Population balances: Theory and applications to particulate systems in engineering. New York: Academic press.

Randolph A.D., Larson M.A. (1964), "A population balance for countable entities". Canadian Journal of Chemical Engineering, 42, 280.

Revankar, S.T., (2001). Coalescence and breakup of fluid particles in multi-phase flow. In: ICMF 2001-4th International Conference on Multiphase Flow, New Oriens, Louisiana, USA, May 27-June 1.

Ross, S.I., (1971). Measurements and models of the dispersed phase mixing process, Ph.D. Dissertation, The University of Michigan, Ann Arbor.

Rotta J.C., (1972), "Turbulente Stromungen", Teubner B.G., Stuttgart.

Saffman, P.G., (1965). The lift on asmall sphere in a slow shear flow.J. Fluid Mech.22, 385-400.

Sari, S., Ergun, S., Barik, M., Kocar, C. and Sokmen, C.N., (2009). Modelling of Isothermal Bubbly Flow with Interfacial Area Transport Equation and Number Density Approach, Annals of Nuclear Energy, 36, 222-232.

Sato Y., Sadatomi M., Sekoguchi K., (1981). "Momentum and Heat Transfer in Two-Phase Bubbly Flow- I". International Journal of Multiphase Flow, 7, 167.

Scott W.T. (1968). Analytic studies of cloud droplet coalescence. Journal of the Atmospheric Science, 25, 54-65.

Serizawa, A., Kataoka, I., and Michiyoshi, I., (1986). Phase Distribution in Bubbly Flow-Data set No. 24, Proceedings of the Second International Workshop on Two-Phase Flow Fundamentals, Troy, NY, USA.

Shinnar, R., Church, J.M., (1960). Predicting Particle Size in Agitated Dispersions. Industrial and Engineering Chemistry 52, 253-256.

Simon, L., (2000). Application of Population Balance to CFD Modelling of Gas-Liquid Reactors, "Trends in Numerical and Physical Modeling for Industrial Multiphase Flows", Corse.

Sokolichin, A. and G. Eigenberger (1999). "Applicability of the Standard $k-\varepsilon$ Turbulence model to the Dynamic Simulation of Bubble Columns: Part I. Detail Numerical Simulations."Chemical Engineering Science 54(13-14): 2273-2284.

Sokolichin, A. and G. Eigenbergen, (1999). "Applicability of the Standard K-Epsilon Turbulence Model to the Dynamic Simulation of Bubble Columns: Part I. Detail Numerical Simulations"' Chem. Eng. Sci. 54, 2273-2284.

Sovova, H., (1981). Breakage and Coalescence of Drops in a Batch Stirred Vessel-Π Comparison of Model and Experiments. Chemical Engineering Science 36, 1567-1573.

Stephen Yamoah, Raúl Martínez-Cuenca, Guillem Monrós, Sergio Chiva, Rafael Macián-Juan (2015). Numerical Investigation of Models for Drag, Lift, Wall Lubrication and Turbulent Dispersion Forces for the Simulation of Gas–Liquid Two-Phase Flow. Chemical Engineering Research and Design Volume 98, June 2015, Pages 17–35.

Sundaresan, S., (2000) "Modelling the Hydrodynamics of Multiphase Flow Reactors: Current Status and Challenges", AIChe J. 46, 1102-1105.

Takagi, S., Ogasawara, T., Matsumoto, Y., (2008). The effects of Surfactant on the Multi-Scale Structure of Bubbly flows. Philos. Trans. Roy.Soc. A 366 (1873), 2117-2129.

Tatterson (1994) G.B., Scale up and Design of Industrial Mixing Processes, Mc Graw Hill, New York.

Tomiyama, A., Sou, A., Zun, A., Kanami, I., Sakaguchi, T., (1995). Effects of *Eötvös* Number and Dimensionless Liquid Volumetric Flux on lateral motion of a Bubble in a Laminar Duct Flow. Advances in Multiphase Flow, Elsevier, 3-15.

Tomiyama A., (1998), "Struggle with computational bubble dynamics", in: Proceeding of the Third international Conference on Multiphase Flow. Lyon, France. Fluid Dynamics Applied to chemical Reaction Engineering", Revue de I'Institut Francais du Petrole, 48, 595-613 (1993).

Trambouze, P., (1993) "Computational Fluid Dynamics Applied to Chemical Reaction Engineering", Revue de I'Institut Francais du Petrole, 48, 595-613.

Troshko, A., Ivanov N. and S. Vasques,(2002) "Implementation of a General Lift Coefficient in the CFD model of Turbulent Bubbly Flows", Fluent Inc., Lebanon, NH.

Tsouris, C., Tavlarides, L, L., (1994). Breakage and Coalescence Models for Drops in Turbulent Dispersions. AIChE Journal 40, 395-406.

Venneker, B.C.H., (2002). Population Balance Modelling of Aerated Stirred Vessels based on CFD. AIChE Journal 48, 673-685.

Vieser, W., Esch, T., Menter, F, (2008). Heat transfer predictions using advanced two-equaton turbulence models, Ansys CFX Validation Report, ANSYS Germany.

Wang, T.F., et al., (2005a). Theoretical prediction of flow regime transition in bubble columns by the population balance model. Chemical Engineering Science 60, 6199-6209.

Wang, T.F., et al., (2005b). Population Balance Model for Gas-Liquid Flows: Influence of Bubble Coalescence and Breakup Models. Industrial and Engineering Chemistry Research 44, 7540-7549.

Wang, T. F., J. F. Wang and Y. Jin (2003). "A Novel Theoretical Breakup Kernel Function for Bubbles/Droplets in a Turbulent Flow. "Chemical Engineering Science 58(20): 4629-4637.

Wu, Q., Kim, S., Ishii, M. and Beus, S. G., (1998). One-Group Interfacial Area Transport in Vertical Bubble Flow. Int. J. Heat Mass Transfer, 41, 1103-1112.

Yamoah, S., (2014). Numerical Modelling of Isothermal Gas Liquid Two-phase Bubbly Flow in Vertical Pipes. Ph.D Dissertation. University of Ghana.

Zhao, Hui and Wei Ge (2007). "A theoretical bubble breakup model for slurry beds or three-phase fluidized beds under high pressure. "Chemical Engineering Science 62(1-2): 109-115.

Ziqi Cai, Yuyun Bao, Zhengming Gao, (2010). Hydrodynamic Behaviour of a Single Bubble Rising in Viscous Liquids, Chinese Journal of Chemical Engineering, Volume 18, Issue 6, Pages 923-930.

Zun, I., (1980). The transverse migration of bubbles influenced by walls in vertical bubbly flow. Int. J. Multiphase Flow 6, 583.

APPENDIX

CFX Expression Language for Case 1

```
Case 1 = factpi1*gammaLe
```

$$F_C = (1-(\exp((Cfact*(((gamma\max Wu)\wedge(1/3)*(GasV1F05)\wedge(1/3))/(((gamma\max Wu)\wedge(1/3))-((GasV1F05)\wedge(1/3)))))*(\exp(-((((gamma\max Le)\wedge(1/3))-((GasV1F05)\wedge(1/3)))/(GasV1F05)\wedge(1/3))))(\wedge 2)$$

```
Cfact1 = 3 []

GasV1F05 = 0.036138 []

gammamaxWu = 0.8 [ ]

gammamaxLe = 0.6 [ ]

factpi1 = 1-(exp((-

Cfact1*(((gammamaxWu)^(1/3)*(GasV1F05)^(1/3))/(((gammamaxWu

)^(1/3))-((GasV1F05)^(1/3)))))))

gammaLe = exp(-(((((gammamaxLe)^(1/3))-

((GasV1F05)^(1/3)))/((GasV1F05)^(1/3)))^(2)))
```

CFX Expression Language for Case 2

```
Case 2 = factpi2*gammaLe
```

$$F_C = \exp(-((((gamma\max Wu)\wedge(1/3)-((GasV1F05)\wedge(1/3)))/((GasV1F05)\wedge(1/3))))*(gamma\max Le)/((gamma\max Le)-(GasV1F05))$$

```
gammaLe = exp(-(((((gammamaxLe)^(1/3))-
((GasV1F05)^(1/3)))/((GasV1F05)^(1/3)))^(2)))
GasV1F05 = 0.036138 []
gammamaxLe = 0.6 [ ]
gammamaxWu = 0.8 [ ]
factpi2 = exp(-((((gammamaxWu)^(1/3))-
((GasV1F05)^(1/3)))/((GasV1F05)^(1/3))))
```

CFX Expression Language for Case 3

```
Case 3 = factpi2*gammaWa
```

$$F_C = (\exp(-((((gamma\max Wu)\wedge(1/3))-((GasV1F05)\wedge(1/3)))/((GasV1f05)\wedge(1/3))))*\exp(-(((gamma\max Wa)\wedge(1/3))-((GasV1F05)\wedge(1/3)))/((GasV1F05)\wedge(1/3)))(\wedge 2)$$

```
GasV1F05 = 0.036138 []
factpi2 = exp(-((((gammamaxWu)^(1/3))-
((GasV1F05)^(1/3)))/((GasV1F05)^(1/3))))
gammaWa = (gammamaxWa)/((gammamaxWa)-(GasV1F05))
```